HHS Public Access

Author manuscript

Sci Transl Med. Author manuscript; available in PMC 2022 April 21.

Published in final edited form as:

Sci Transl Med. 2021 July 28; 13(604): . doi:10.1126/scitranslmed.abe1923.

Nuclear accumulation of CHMP7 initiates nuclear pore complex injury and subsequent TDP-43 dysfunction in sporadic and familial ALS

Alyssa N. Coyne[1,2,*], **Victoria Baskerville**[1], **Benjamin L. Zaepfel**[3], **Dennis W. Dickson**[4], **Frank Rigo**[5], **Frank Bennett**[5], **C. Patrick Lusk**[6], **Jeffrey D. Rothstein**[1,2,*]

[1]Brain Science Institute, Johns Hopkins University School of Medicine, Baltimore, MD 21205, USA

[2]Department of Neurology, Johns Hopkins University School of Medicine, Baltimore, MD 21205, USA

[3]Biochemistry, Cellular, and Molecular Biology Graduate Program, Johns Hopkins University School of Medicine, Baltimore, MD 21205, USA

[4]Department of Neuroscience, Mayo Clinic, Jacksonville, FL 32224, USA

[5]Ionis Pharmaceuticals, Carlsbad, CA 92010, USA

[6]Department of Cell Biology, Yale School of Medicine, New Haven, CT 06520, USA

Abstract

Alterations in the components [nucleoporins (Nups)] and function of the nuclear pore complex (NPC) have been implicated as contributors to the pathogenesis of genetic forms of neurodegeneration including *C9orf72* amyotrophic lateral sclerosis/frontotemporal dementia (ALS/FTD). We hypothesized that Nup alterations and the consequential loss of NPC function may lie upstream of TDP-43 dysfunction and mislocalization widely observed in ALS, FTD, and related neurodegenerative diseases. Here, we provide evidence that CHMP7, a critical mediator of NPC quality control, is increased in nuclei of *C9orf72* and sporadic ALS induced pluripotent stem cell (iPSC)–derived spinal neurons (iPSNs) and postmortem human motor cortex before the emergence of Nup alterations. Inhibiting the nuclear export of CHMP7 triggered Nup reduction and TDP-43 dysfunction and pathology in human neurons. Knockdown of CHMP7 alleviated disease-associated Nup alterations, deficits in Ran GTPase localization, defects in

[*]Corresponding author. jrothstein@jhmi.edu (J.D.R.); acoyne3@jhmi.edu (A.N.C.).

Author contributions: Conceived and designed all experiments: A.N.C. and J.D.R., with critical input and advice from C.P.L. Performed the experiments: A.N.C., with technical assistance (iPSC line maintenance) from V.B. Analyzed all data: A.N.C. and J.D.R., with contributions from B.L.Z. for quantification from postmortem tissues. Contributed reagents and materials for this study: A.N.C. and J.D.R. (all experiments), D.W.D. (postmortem human tissues), and F.R. and F.B. (ASOs). Wrote the manuscript: A.N.C. and J.D.R., with editing from coauthors.

SUPPLEMENTARY MATERIALS http://stm.sciencemag.org/content/suppl/2021/07/26/13.604.eabe1923.DC1

View/request a protocol for this paper from Bio-protocol.

Data and materials availability: All data associated with this study are present in the paper or the Supplementary Materials. Requests for materials should be addressed to J.D.R. (jrothstein@jhmi.edu). ASOs used in this study can be obtained from Ionis Pharmaceuticals (F.B., fbennett@ionisph.com) under a standard research material transfer agreement.

TDP-43-associated mRNA expression, and downstream glutamate-induced neuronal death. Thus, our data support a role for altered CHMP7-mediated Nup homeostasis as a prominent initiating pathological mechanism for familial and sporadic ALS and highlight the potential for CHMP7 as therapeutic target.

INTRODUCTION

The motor neuron disease amyotrophic lateral sclerosis (ALS) is a devastating neurodegenerative disease affecting multiple neuronal and glial subtypes within the motor cortex and spinal cord. About 10% of ALS cases are familial (fALS), with mutations in more than 20 genes identified to date. The most common genetic cause of ALS is a hexanucleotide repeat expansion in the *C9orf72* gene, accounting for about 40% of fALS and 8% of sporadic ALS (sALS). However, 90% of ALS cases are sALS with no known underlying causative genetic mutation. Despite the heterogeneous nature of ALS etiology, nuclear clearing and cytoplasmic mislocalization and/or aggregation of TAR DNA binding protein (TDP-43) has emerged as a prominent pathological hallmark of end-stage familial and sporadic disease (1–3).

Although studies of genetic forms of ALS including *C9orf72* have provided important insights into underlying disease mechanisms and potential therapeutic strategies, these discoveries do not necessarily translate to sALS. The lack of preclinical animal model systems that faithfully reproduce the heterogeneous nature of human sALS highlights a major challenge in understanding 90% of ALS pathophysiology. However, the reprogramming of patient-derived fibroblasts and peripheral blood mononuclear cells (PBMCs) into induced pluripotent stem cells (iPSCs) allows for the controlled differentiation into neuronal and glial cells to model human disease (4, 5). Studies from our laboratory and others have shown that *C9orf72* iPSC-derived motor neurons (iPSNs) recapitulate key pathological features of disease seen in postmortem human central nervous system (CNS) tissues (6, 7). As a result, iPSNs provide a useful and relevant platform for studying mechanisms underlying ALS and other neurodegenerative diseases.

Molecular changes to the composition of the nuclear pore complex (NPC) have been identified as an early and key pathomechanism in *C9orf72* disease (8). The NPC is composed of multiple copies of ~30 distinct nucleoporins (Nups) organized into subcomplexes. Scaffold Nups build the eightfold radial architecture of the NPC and secure it to the nuclear envelope. The NPC scaffold provides anchor points for FG-Nups that fill the central transport channel and mediate the nucleocytoplasmic exchange of macromolecules. Some Nups can also function in pools outside the NPC as part of the mitotic apparatus and within the nucleoplasm where they affect gene transcription (9–12). Given the critical roles of the NPC in maintaining overall cellular function, alterations in specific Nups may affect neuronal viability and give rise to disease pathology. Our recent study revealed that a specific subset of eight Nups, beginning with POM121, is substantially reduced within the NPC and nucleoplasm of *C9orf72* iPSN and postmortem human neuronal nuclei. The collective reduction in these eight specific Nups from the nucleoplasm and NPCs of *C9orf72* human neurons affects nucleocytoplasmic transport (NCT) and neuronal survival without

alterations to Nup mRNA metabolism (8). Collectively, these data suggest that substantial and early alterations in Nup protein homeostasis may underlie reduction of Nups in *C9orf72* ALS/frontotemporal dementia (FTD) pathogenesis. However, the molecular pathway that underlies human neuronal NPC disruption and whether this pathophysiology is more broadly applicable to sporadic disease remain unknown.

Work in several model systems supports the existence of molecular pathways that can affect Nup and NPC homeostasis within the nuclear envelope and nucleoplasm. For example, in budding yeast, the recruitment of the endosomal sorting complexes required for transport (ESCRT) machinery by LEM family inner nuclear membrane (INM) proteins has been implicated in the proteasomal degradation of misassembled Nups (13) and the sealing of defective NPCs (14, 15). Analogous mechanisms likely function in nonneuronal mammalian cells to facilitate the removal of Nups and NPCs (16). Recent work in yeast reveals that both individual Nups and NPCs can also be targets of autophagy (17, 18). Critically, the nuclear recruitment and/or retention of the ESCRT-III protein CHMP7 appears to be an initiating step in proper Nup and NPC homeostasis (14, 15, 19). Under normal cellular conditions, CHMP7 is predominantly localized to the cytoplasm. Recent reports suggest that, in nonneuronal cells, CHMP7 continually passively diffuses into the nucleus in a LEMD2-dependent manner. Active nuclear export via Exportin-1 (XPO1,CRM1) ensures that nuclear CHMP7 expression remains low (13–15), thereby preventing nuclear accumulation in the absence of nuclear injury. However, little is known regarding CHMP7-mediated Nup proteostasis in human neurons and its impact on NPC and nucleoplasm Nup abundance in neurodegeneration.

Using iPSNs and postmortem human tissue, we show that CHMP7 expression is elevated in *C9orf72* and sALS nuclei. Mechanistically, impaired nuclear export of CHMP7 leads to reduced expression of specific Nups, alterations in *STMN2* splicing, and TDP-43 mislocalization in human neurons. Antisense oligonucleotide (ASO)–mediated knockdown of CHMP7 mitigated the reduction of specific Nups from the nucleoplasm and NPCs in *C9orf72* iPSNs. CHMP7 ASOs additionally alleviated defects in mRNA expression associated with loss of TDP-43 and downstream neuronal toxicity. Collectively, these data suggest that, in human neurons, aberrant nuclear expression and localization of CHMP7 is a substantial and early contributor to Nup alterations in ALS. In addition, our data highlight the potential for CHMP7 as a therapeutic target in familial and sporadic ALS/FTD and related neurodegenerative diseases characterized by Nup reduction and TDP-43 pathology.

RESULTS

Specific Nups are reduced in sALS iPSN nuclei

Recently, we established that decreased expression of the transmembrane Nup POM121 affects the expression of seven additional Nups spanning multiple subcomplexes of the NPC (8). Given that multiple pathologies and molecular pathways are commonly linked to both familial and sporadic ALS (1, 3, 20), we hypothesized that Nup reduction may also be a prominent pathological feature in sporadic disease. Therefore, on the basis of our previous studies in *C9orf72* ALS/FTD, we selected a subset of candidate Nups spanning multiple subcomplexes of the NPC and visually examined their nuclear distribution and expression

using super-resolution structured illumination microscopy (SIM) in nuclei isolated from control and sALS iPSNs. SIM is capable of providing an estimated resolution of 100 nm, approximating the dimensions of an individual human NPC (10, 21, 22), thus allowing us to evaluate the NPC localization and expression of Nups. Using this methodology, we found that a subset of Nups is reduced from the nucleoplasm and NPCs of NeuN-positive sALS iPSN nuclei (Fig. 1, A and B). In contrast, we observed no overt changes to the distribution or expression of the various FxFG-rich Nups recognized by mAb414 (414; Fig. 1, A and B). The pathological reduction in Nup50, TPR, POM121, and Nup133 in sALS neuronal nuclei (Fig. 1, A and B) was similar to that detected in *C9orf72* nuclei (8). None of the sALS iPSC lines evaluated tested positive for known genetic mutations associated with ALS (for more information, see Materials and Methods and dataportal.answerals.org). Together, these data suggest that common molecular events may underlie Nup reduction in familial and sporadic disease.

The nuclear expression and localization of CHMP7 are increased in C9orf72 and sALS iPSNs and postmortem human motor cortex

Given the critical involvement of CHMP7 in NPC homeostasis in yeast (13–15), we investigated whether the expression of this protein was pathologically altered in *C9orf72* and sALS nuclei. Using SIM, we found a drastic increase in CHMP7 immunoreactivity in NeuN-positive nuclei isolated from control and *C9orf72* and sALS iPSNs (Fig. 1, C and D). We also observed an increase in the number of CHMP7 spots in NeuN-positive nuclei isolated from C9orf72 and sALS postmortem motor cortex (fig. S1), thus confirming that our iPSN model system recapitulates true human pathology. Although CHMP7 does rarely localize in close proximity to Nup62-positive NPCs and spots, its increased expression, as evaluated by immunostaining with two independent antibodies, appears predominantly nucleoplasmic in *C9orf72* and sALS iPSNs (fig. S2). In addition, Western blot analyses using two different anti-CHMP7 antibodies quantitatively confirmed an increase in CHMP7 protein abundance in *C9orf72* and sALS nuclei (Fig. 1, E to G). This increase was observed even at a time point (day 18 of differentiation; Fig. 1, C and D) preceding that at which Nup reduction was observed (day 32; Fig. 1, A and B) (8). We have previously reported that NPC injury can be initiated by Trim21-mediated degradation (23) of the transmembrane Nup POM121 (8). Here, we found that rapid reduction of endogenous POM121 from wild-type iPSN nuclei did not result in increased nuclear CHMP7 expression (fig. S3). Together, these data suggest that CHMP7 is not responding to NPC injury but may play a more direct role in its initiation.

Because the nuclear/cytoplasmic partitioning of multiple proteins is disrupted in multiple neurodegenerative diseases (24–27), we next evaluated the nuclear and cytoplasmic distribution of CHMP7 in our ALS iPSNs. Using immunostaining and confocal imaging, we observed a robust relocalization of CHMP7 from the cytoplasm to the nucleus in *C9orf72* and sALS iPSNs (Fig. 2, A and B). Consequently, similar to our observations in isolated nuclei (Fig. 1, C and D), this corresponded to an increase in overall anti-CHMP7 nuclear immunoreactivity in *C9orf72* and sALS iPSNs compared to controls (Fig. 2, A and C). Consistent with a relocalization of CHMP7 protein from the cytoplasm to the nucleus, we did not observe changes in total CHMP7 protein abundance in *C9orf72* or

sALS iPSN lysates (fig. S4). To further verify that our results in iPSNs recapitulated human disease pathology, we performed immunostaining in thin paraffin-embedded sections from postmortem motor cortex. Compared to nonneurological controls, there was a substantial relocalization of CHMP7 to the nucleus (Fig. 2, D and E) and overall increase in CHMP7 nuclear intensity (Fig. 2, D and F) in Map2-positive neurons in *C9orf72* and sALS motor cortex mimicking our data obtained in iPSNs. Using two orthogonal approaches, SIM and immunostaining of thin paraffin-embedded sections, we did not observe a similar increase in nuclear CHMP7 immunoreactivity in the occipital cortex, a brain region unaffected in ALS (figs. S1 and S5). Together, this suggests that nuclear accumulation of CHMP7 is specific to neurons affected in ALS pathogenesis.

Impaired nuclear export of CHMP7 recapitulates disease-associated reduction in specific Nups

Having established that increased nuclear CHMP7 is a robust and prominent molecular feature of sALS and fALS/FTD, we next sought to determine the mechanism by which this pathology occurred in human neuronal nuclei. In both yeast and human cells, CHMP7 cannot accumulate in the nucleus because of its active nuclear export by XPO1/CRM1 (14, 28). It is thought that perturbations to the nuclear envelope, either to the nuclear membranes themselves or to NPCs, leads to CHMP7 entry into the nucleus, where it triggers an NPC surveillance pathway (19). However, as CHMP7 accumulates in the nucleus before Nup reduction in iPSNs, we wondered whether this aberrant nuclear accumulation of CHMP7 might be a cause, not a consequence, of Nup reduction. To test this idea, we mimicked CHMP7 nuclear accumulation by overexpressing an allele of CHMP7 with a specific mutation (L to A, amino acid 430) in its NES that abrogates XPO1 binding, thereby allowing this CHMP7 NES* mutant to access the nucleoplasm. Overexpression of GFP-tagged CHMP7 NES*, but not wild-type GFP–tagged CHMP7, in wild-type iPSNs (Fig. 3, A and B) recapitulated *C9orf72* and sALS disease-associated reductions of Nup50, POM121, and Nup133 abundance, as evaluated by SIM (Fig. 3, A and C to F). Consistent with a role for CHMP7 as an early-acting factor that mediates Nup and NPC degradation (13–15), these data suggest that artificially induced nuclear accumulation of CHMP7 is sufficient to facilitate alterations to Nup expression in iPSN nuclei. In otherwise wild-type iPSNs, overexpression of wild-type CHMP7 was not sufficient to promote its nuclear accumulation (Figs. 3, A and B, and 4A). This is likely due to the continued normal regulation of CHMP7's passive diffusion into and active XPO1-mediated export out of the nucleus (13–15, 28). Therefore, nuclear CHMP7 abundance remains low in wild-type iPSNs overexpressing a wild-type CHMP7 variant that is subject to typical regulation of CHMP7 localization.

Both the yeast and human CHMP7 orthologs are recruited to the nuclear envelope by the integral INM protein LEMD2 in nonneuronal cell types (15, 29). As we do not observe any obvious nuclear envelope accumulation of CHMP7 in iPSNs (fig. S2), we hypothesized that CHMP7's interaction with LEMD2 was not required in this context. Neither a reduction in endogenous LEMD2 (fig. S6, A and B) nor overexpression of GFP-tagged LEMD2 had an effect on nuclear CHMP7, POM121, or mAb414 nuclear immunoreactivity (fig. S6, C to L).

Impaired nuclear export of CHMP7 leads to TDP-43 mislocalization and altered mRNA expression

As overexpression of CHMP7 NES* could recapitulate Nup reduction in otherwise wild-type iPSNs, we considered whether this aberrant CHMP7 localization might also trigger other ALS-associated phenotypes and pathologies. For example, TDP-43 is a DNA and RNA binding protein that is localized predominantly in the nucleus. However, within a subset of neurons in ~97% of ALS cases, TDP-43 is cleared from the nucleus and/or mislocalized (and in some cases subsequently aggregated) in the cytoplasm. It is believed that this nuclear clearing, thought to occur before cytoplasmic aggregation (30, 31), leads to a loss of TDP-43 function and is a pathogenic event in multiple neurodegenerative diseases including sALS (1, 32). However, the mechanisms that contribute to a reduction in nuclear TDP-43 expression remain poorly understood. Given that TDP-43 shuttles between the nucleus and cytoplasm to regulate the metabolism of its mRNA targets (30, 33), we hypothesized that perhaps CHMP7-mediated NPC injury may at least, in part, contribute to TDP-43 mislocalization and dysfunction in human neurons. To test this, we first overexpressed GFP-tagged CHMP7 variants in wild-type iPSNs and monitored the localization of endogenous TDP-43 via immunostaining and confocal microscopy.

A week after Nup alterations were first observed (Fig. 3), overexpression of wild-type CHMP7 had no effect on the subcellular localization of endogenous TDP-43, which remained in the nucleus (Fig. 4, A to C). In contrast, overexpression of CHMP7 NES* resulted in a relocalization of TDP-43, establishing a visible cytosolic pool of TDP-43 (Fig. 4A). This was further quantified as a nuclear/cytoplasmic ratio and overall anti–TDP-43 nuclear fluorescence. Whereas the nuclear/cytoplasmic ratio was strongly decreased from 10.7 to 1.9, nuclear TDP-43 immunoreactivity was more subtly reduced in GFP-tagged CHMP7 NES*–overexpressing cells (Fig. 4, A to C). To evaluate the functional consequence of this change in TDP-43 distribution, we took advantage of recent work, indicating that alterations in *STMN2* mRNA splicing are a prominent pathological consequence of loss of nuclear TDP-43 function (34–36). We therefore performed quantitative reverse transcription polymerase chain reaction (qRT-PCR) for full-length and truncated *STMN2* mRNA species in the context of CHMP7 and CHMP7 NES* overexpression. Consistent with the interpretation that mislocalization of TDP-43 affects its function, overexpression of CHMP7 NES*, but not GFP or wild-type CHMP7, reduced the total abundance of full-length *STMN2* mRNA with a corresponding increase in truncated *STMN2* mRNA (Fig. 4, D and E). As an additional readout of TDP-43 functionality, we performed qRT-PCR for four additional mRNAs (*ELAVL3, PFKP, RCAN1*, and *SELPLG*) previously shown to decrease in abundance upon knockdown of TDP-43 in iPSNs (36). Similar to our observations for *STMN2* mRNA, overexpression of CHMP7 NES*, but not wild-type CHMP7, substantially reduced the abundance of *ELAVL3, PFKP, RCAN1*, and *SELPLG* mRNAs compared to GFP overexpression (fig. S7). Together, these data indicate that nuclear accumulation of CHMP7 is sufficient to trigger a pathological cascade affecting nuclear Nup expression and TDP-43 localization and function in human neurons.

Next, to investigate whether CHMP7 and TDP-43 co-pathology could be observed in real human disease, we performed double immunostaining in thin paraffin-embedded sections

from postmortem nonneurological control, *C9orf72* ALS/FTD, and sALS motor cortex (Fig. 5A). Nuclear CHMP7 immunoreactivity remained low, supporting our previous analyses (Fig. 2, D to F), and as expected, TDP-43 was predominantly localized to the nucleus in the majority of neurons in motor cortex from nonneurological control patients. Consistent with reports that TDP-43 mislocalization can occasionally be observed in normal aging (37) or as a result of nondegenerative neuronal injury (38, 39), a small subset of neurons in nonneurologic control motor cortex tissue displayed a decreased nuclear/cytoplasmic TDP-43 immunoreactivity independent of CHMP7 pathology (Fig. 5B, blue box). In contrast, we found that about 80 to 90% of Map2-positive neurons in *C9orf72* and sALS patient motor cortex display increased nuclear CHMP7 immunostaining (Fig. 5), in agreement with our earlier analyses (Fig. 2, D to F). A substantial subset of these CHMP7 pathology–positive neurons also displayed a decreased nuclear/cytoplasmic ratio of TDP-43 immunostaining (Fig. 5, A, C, and D). Cytoplasmic TDP-43 aggregation was observed in a handful of neurons with decreased cytoplasmic/nuclear CHMP7 immunoreactivity (Fig. 5A). A large portion of the neurons evaluated were positive for CHMP7 pathology but negative for TDP-43 pathology (Fig. 5, A, C, and D), consistent with our hypothesis that increased nuclear CHMP7 is an early and prominent event in neuronal injury in neurodegeneration.

ASO-mediated knockdown of CHMP7 mitigates Nup alterations, alleviates deficits in mRNA expression associated with TDP-43 loss of function, and improves neuronal survival

Given our data suggesting that increased nuclear abundance of CHMP7 can affect Nup expression and TDP-43 localization and function, we hypothesized that therapeutically reducing CHMP7 could prove beneficial for neurodegenerative disease characterized by Nup alterations and TDP-43 dysfunction. ASOs are now used as a therapeutic strategy to reduce mRNA and protein expression of genes of interests (40, 41). To determine whether reducing CHMP7 would effectively mitigate NPC injury, ASOs were designed to specifically target human CHMP7 pre-mRNA and induce its degradation via ribonuclease H–based mechanisms. Compared to scrambled control ASOs, 2-week exposure to three different CHMP7 targeting ASOs substantially reduced CHMP7 protein expression in control, *C9orf72*, and sALS iPSNs in a dose-dependent manner (fig. S8). Consistent with our Western blot experiments using whole iPSN lysates (fig. S8), SIM analyses revealed that CHMP7 ASO treatment reduced nuclear abundance of CHMP7 in control, *C9orf72*, and sALS iPSNs (Fig. 6, A and B). Moreover, compared to a scrambled control ASO, 5 μM CHMP7 ASO 2 restored POM121, Nup133, and Nup50 expression in *C9orf72* and sALS iPSN nuclei and NPCs (Fig. 6, A and C to F), as evaluated by SIM. Consistent with our results in isolated nuclei, CHMP7 ASO treatment restored the nuclear expression of POM121, Nup133, and Nup50 in intact iPSNs (fig. S9). We did not observe any disruption in Nups in control iPSNs treated with CHMP7 ASOs (Fig. 6, A and C to F) or mAb414 immunoreactivity in *C9orf72* or sALS iPSNs (Fig. 6, A and F), suggesting that ASO-mediated knockdown of CHMP7 protein specifically mitigates disease-associated Nup alterations in iPSNs.

Ran guanosine triphosphatase (GTPase) must be maintained at high concentrations within the nucleus to provide sufficient energy to power bidirectional NCT through the NPC

(11, 42). We have previously shown that restoration of nuclear Nup expression restores the localization of Ran GTPase to the nucleus in *C9orf72* iPSNs (8). Consistent with this report, knockdown and CHMP7, and subsequent restoration of Nup expression within the nucleoplasm and NPC, restored the proper subcellular distribution of Ran GTPase in *C9orf72* and sALS iPSNs (fig. S10).

To determine whether ASO-mediated knockdown of CHMP7 was sufficient to mitigate TDP-43–mediated splicing dysfunction, we performed qRT-PCR for full-length and truncated *STMN2* mRNAs. At day 46 of differentiation, about 2 weeks after the emergence of nuclear Nup reduction, we observed a substantial decrease in full-length *STMN2* mRNA and a corresponding increase in truncated *STMN2* mRNA in scrambled control ASO–treated *C9orf72* and sALS iPSNs (Fig. 6, G and H). After 3-week exposure to CHMP7 ASO 2, 1 week longer than was necessary to restore Nup expression, full-length and truncated *STMN2* mRNA abundance were restored (Fig. 6, G and H). Consistent with a reversal of defects in RNA metabolism associated with TDP-43 loss of function in iPSNs, 3-week exposure to CHMP7 ASO 2 restored the abundance of *ELAVL3, PFKP, RCAN1*, and *SELPLG* mRNAs in *C9orf72* and sALS iPSNs (fig. S11).

Although we did not observe TDP-43 mislocalization in *C9orf72* iPSNs (fig. S12), consistent with our previous study (8), a clear “molecular signature” of TDP-43 loss of function is exemplified by defects in mRNA metabolism (Fig. 6, G and H, and fig. S11). This suggests that molecular hallmarks of TDP-43 loss of function may be observed before overt protein mislocalization. Nonetheless, in a subset of sALS iPSC lines evaluated, we did observe a subtle mislocalization of TDP-43 from the nucleus to the cytoplasm at day 46 of differentiation (fig. S12). Consistent with a role in mitigating loss of TDP-43 function, 3-week treatment with CHMP7 ASO 2 restored nuclear TDP-43 localization in sALS iPSNs (fig. S11).

The combinatorial effects of our observed Nup alterations are likely to affect multiple cellular functions and pathways critical to neuronal survival. As a result, we next evaluated the efficacy of CHMP7 ASOs in alleviating deficits in stressor-induced neuronal survival. Two-week treatment with CHMP7 ASO 2 decreased the sensitivity of *C9orf72* and sALS iPSNs to glutamate-induced excitotoxicity (Fig. 6I and fig. S13), as measured by propidium iodide (PI) incorporation, a well-established assay to measure neuronal sensitivity to stress (6, 8). CHMP7 ASO treatment itself was not neurotoxic (0 μM glutamate; Fig. 6I and fig. S13). Together, these data highlight the therapeutic potential for CHMP7 ASOs in mitigating Nup and NPC defects, TDP-43 dysfunction, and downstream neuronal death in *C9orf72* and sALS iPSNs.

DISCUSSION

Pathological Nup alterations are prevalent in multiple neurodegenerative diseases including ALS, Alzheimer’s disease (AD), and Huntington’s disease (HD) (43–46). However, the molecular mechanisms by which these disruptions occur remain poorly understood. In contrast to the cytoplasmic Nup mislocalization observed in artificial overexpression mouse models of *C9orf72* ALS/FTD (47–50), we have previously shown that, in human neurons,

there is a reduction in the NPC and nucleoplasmic expression of eight specific Nup proteins spanning multiple subcomplexes of the NPC without corresponding cytoplasmic accumulations (8). As a result, we hypothesized that altered Nup surveillance and homeostasis may contribute to reduced Nup expression in *C9orf72* and sALS iPSNs.

Recent work in yeast and nonneuronal cellular systems has identified CHMP7 as important mediator of NPC, Nup, and nuclear envelope homeostasis (13, 15,16, 51). However, the contribution of this pathway to neuronal biology and disease pathophysiology is unknown. Using an iPSN model of sALS and fALS/FTD, we provide evidence that disease-associated increased nuclear CHMP7 expression contributes to reduced nuclear abundance of key Nups located within three distinct domains of the NPC as an early event in disease pathogenesis. Nuclear accumulation of CHMP7 does not appear to be responding to NPC injury but instead triggers Nup reduction in iPSNs. In human neurons, the INM protein LEMD2 does not appear to affect the nuclear localization of CHMP7. However, the possibility remains that the nuclear envelope itself or another nuclear protein mediates CHMP7 nuclear accumulation in ALS iPSNs. Nonetheless, our data define a functional role for CHMP7-mediated Nup homeostasis in human neurons and neurodegeneration.

A direct role for other ESCRT proteins in the removal of proteins from membranes has previously been defined (52, 53). However, it remains unclear as to whether CHMP7 itself can function similarly. Further, both proteasomal and lysosomal (autophagy) degradation pathways have been linked to ESCRT-III–mediated Nup proteostasis (13–18). Ongoing work is poised to address these critical questions and further our understanding of the role of CHMP7 in the initiation of early pathogenic events in ALS.

Although ESCRT-III–mediated NPC and nuclear envelope repair are initiated by the ESCRT-III adapter protein CHMP7 (52), the recruitment and involvement of other CHMPs in this process remain unknown in multiple cellular systems including human neurons. Given that mutations in the ESCRT-III pathway component CHMP2B have been implicated in FTD (54), it will be interesting to evaluate whether or not these mutations are sufficient to induce Nup reduction in a manner similar to that observed in *C9orf72* and sALS iPSNs.

The nuclear clearance and mislocalization of TDP-43 is regarded as a prominent neuropathological hallmark of all sALS and related neurodegenerative diseases, including a substantial subset of AD and FTD (1, 37, 55–61). However, the biological events that may contribute to TDP-43 loss of function or pathology are poorly understood. We now provide multiple lines of evidence that nuclear retention of CHMP7 can at least, in part, contribute to TDP-43 mislocalization and dysfunction in disease. Altered TDP-43 localization and deficits in mRNA metabolism occur at time points well after the emergence of Nup alterations in *C9orf72* and sALS iPSNs and control iPSNs artificially overexpressing a nuclear retained CHMP7. These data support our pathology analyses whereby 80 to 90% of postmortem disease neurons display increased CHMP7 immunoreactivity, with a subset of those that are also positive for TDP-43 pathology. Although the precise molecular events that occur after Nup reduction and ultimately lead to TDP-43 pathology remain unknown, our data provide evidence that CHMP7-mediated NPC injury is sufficient to initiate TDP-43 loss of function in ALS.

Although this is the largest study of individual sALS patient–derived iPSC lines to date, it is possible that pathogenic manifestations in subsets of sALS patients may be independent of CHMP7 pathology and/or NPC injury. In addition, we have not yet determined whether CHMP7 pathology and NPC injury are also present in ALS patients with prominent FTD. Last, the core reason for investigating disease mechanisms of sALS in a large set of iPSC lines is that mouse models of authentic sALS do not yet exist. However, future development of new rodent models may enhance our ability to study this NPC injury cascade and therapeutic modulation of CHMP7 in vivo.

Collectively, our data suggest that increased nuclear CHMP7 is a critical initiator of pathogenic cascades affecting the nuclear abundance of specific Nups spanning multiple subcomplexes of the neuronal NPC within *C9orf72* and sALS nuclei. Ultimately, this combined “injury” to the NPC appears to contribute to TDP-43 dysfunction and downstream deficits in neuronal survival. Thus, our data link a new pathophysiological disease pathway, the aberrant nuclear accumulation of CHMP7, to the known prominent pathological hallmark of multiple neurodegenerative diseases, TDP-43 mislocalization and dysfunction. Moreover, our data highlight CHMP7 as a potential therapeutic target in neurodegenerative diseases characterized by nuclear Nup reduction and TDP-43 pathology.

MATERIALS AND METHODS

Study design

The goals of this study were to (i) evaluate CHMP7 pathology in *C9orf72* and sALS, (ii) determine the contribution of CHMP7 pathology to Nup alterations and downstream cellular dysfunction (Ran GTPase localization, TDP-43 function and localization, and neuronal response to glutamate stressors), and (iii) investigate the therapeutic efficacy of CHMP7 ASOs in iPSNs. The primary analyses in our study were to (i) use SIM and confocal microscopy to evaluate CHMP7 pathology Nup alterations in iPSNs and postmortem human CNS tissues and (ii) employ confocal microscopy and qRT-PCR to evaluate downstream consequences of NPC injury. Our analysis was carried out using nonneurological control, *C9orf72*, and sALS (with no known causative genetic mutations) iPSC lines and postmortem tissues. Sample size for postmortem studies was based on availability of high-quality tissue samples. For iPSN experiments, sample sizes were chosen on the basis of previous expertise, knowledge from past experiments, and statistical considerations using similar iPSC-derived motor neuron model systems and current accepted standards based on journal policies and a review of the literature. No statistical analysis was used to predetermine sample size. Sample sizes were chosen to be similar or exceed those previously reported in the literature. Each experiment was repeated with multiple biological replicates as stated, and the statistical analysis demonstrates that our sample sizes revealed significant differences between groups. All experiments were done with a minimum number of replicates based on previous expertise in statistical analyses of similar experimental datasets. No data were excluded from the study. The findings in this study were collected from multiple independent experiments and were reliably reproduced. The number of independent iPSC lines or postmortem tissue samples is indicated in each figure legend. Investigators were blinded to iPSC line and genotypic information for all imaging and quantitative analysis of

all images (SIM, confocal, human tissue, etc.) presented in this study. iPSCs were tested for pluripotency by Cedars-Sinai iPSC Core. iPSNs were validated with known neuronal markers. *C9orf72* repeat expansion was confirmed by Southern blot and qRT-PCR. All cell lines routinely tested negative for mycoplasma contamination. iPSC lines were available through the Answer ALS Project and obtained via the Cedars-Sinai iPSC repository (https://biomanufacturing.cedars-sinai.org). Human nonneurologic control, *C9orf72*, and sALS CNS tissues were available from the Target ALS Postmortem Tissue Core and D. Dickson (Mayo Clinic). For Target ALS specimens, a web-based searchable database of the postmortem tissue inventory provides estimates of fixed and frozen postmortem tissues available that meet basic demographic criteria. Eligible patients and/or family members are recruited from our ALS clinic for voluntary participation in blood and autopsy donations. All blood (for iPSC generation from PBMCs) and autopsied tissue collections are Johns Hopkins Institutional Review Board–approved with Johns Hopkins ethics oversight. All patient information is Health Insurance Portability and Accountability Act (HIPAA) compliant.

iPSC-derived neuronal differentiation

C9orf72, sALS, and nonneurological control iPSC lines were obtained from the Answer ALS repository at Cedars-Sinai (see table S1 for demographics). All sALS iPSC lines are negative for the *C9orf72* repeat expansion and other known ALS mutations. See dataportal.answerals.org for more information on ALS mutations and genetic variants for all iPSC lines used in this study. Feeder-free iPSCs were maintained on Matrigel with MTeSR and maintained according to Cedars-Sinai Standard Operating Procedure (SOP, https://www.cedars-sinai.edu/content/dam/cedars-sinai/research/documents/biomanufacturing/complete-ipsc-culturing-protocol-rev-4-2020.pdf). iPSCs were differentiated into spinal neurons using the previously described direct induced motor neuron protocol (8). All cells were maintained at 37°C with 5% CO_2. iPSCs and iPSNs routinely tested negative for mycoplasma.

ASO treatment of iPSC-derived neurons

Nontargeting scrambled control (676630) (CCTATAGGACTATCCAGGAA), CHMP7 ASO 1 (1508916) (GAAAACGGTTTCCACTGTAT),CHMP7 ASO 2 (1508917) (TGTTACCCTCAGATACCGCC), and CHMP7 ASO 3 (1508918) (ATGTGATGCTATTAATAGGA) were provided by Ionis Pharmaceuticals. On day 25 of differentiation, ASOs were added to the culture media at concentrations of 1, 5, or 10 μM as indicated in figure legends. Medium was exchanged and ASO was replaced every 3 days until iPSNs were subjected to downstream analyses on day 40 of differentiation for Western blot, SIM, and glutamate excitotoxicity and on day 46 of differentiation for qRT-PCR, Ran GTPase localization, and TDP-43 localization.

Nuclei isolation

Nuclei were isolated from iPSNs and postmortem human brain tissue using the Nuclei Pure Prep Nuclei Isolation Kit (Sigma-Aldrich) following the manufacturer's protocol as previously described (8). Briefly, iPSN lysates were prepared by rinsing iPSNs with 1× phosphate-buffered saline (PBS), adding supplied lysis buffer supplemented with dithiothreitol and Triton X-100 directly to each well, and harvesting iPSNs with a cell

scraper. Lysates were transferred to a 50-ml conical tube and vortexed. Sucrose gradients were assembled following the manufacturer's protocol. A 1.85 M sucrose gradient was used to enrich for neuronal nuclei. Samples were centrifuged at 15,600 rpm and 4°C using a Swi32T swinging bucket rotor and Beckman ultracentrifuge (Beckman Coulter) for 45 min. The supernatant was discarded, and the remaining nuclei pellet was resuspended in 1 ml of supplied nuclei storage buffer to wash the nuclei of any remaining sucrose. Resuspended nuclei were centrifuged at 2500 rpm and 4°C for 5 min. The supernatant was once again discarded, and the resulting nuclei pellet was vortexed in 1 ml of supplied nuclei storage buffer to resuspend for downstream imaging analysis. For Western blots, washed nuclei were lysed in radioimmunoprecipitation assay (RIPA) buffer as described below.

Super-resolution SIM

Nuclei staining and super-resolution imaging were performed as previously described (8). After nuclei isolation, 10 to 50 μl of final nuclei/storage buffer suspension were centrifuged onto collagen-coated (1 mg/ml; Advanced Biomatrix) slides with a CytoSpin 4 centrifuge (Thermo Fisher Scientific). Nuclei were immediately fixed with 4% paraformaldehyde (PFA) for 15 min, washed with 1× PBS three times for 10 min, and permeabilized with 1× PBS containing 0.1% Triton X-100 (PBST) for 15 min. Nuclei were then blocked with 10% normal goat serum diluted in 1× PBS for 1 hour at room temperature and incubated in primary antibody diluted in block (10% normal goat serum in 1× PBS) overnight at 4°C (see table S2 for antibody information). After 16 to 18 hours, nuclei were washed with 1× PBS three times for 10 min and incubated in secondary antibody diluted in block (10% normal goat serum in 1× PBS) for 1 hour at room temperature (see table S2 for antibody information). Nuclei were washed with 1× PBS three times for 10 min and coverslipped using Prolong Gold Antifade Reagent (Invitrogen) and 18 mm × 18 mm 1.5 high tolerance coverslips (MatTek).

NeuN- or GFP-positive nuclei (see figure legends) were identified via microscope eye pieces. A single z section ~110 nm thick was acquired by widefield imaging to confirm NeuN or GFP positivity. The immunostained proteins were subsequently imaged by super-resolution SIM using a Zeiss ELYRA S1. For each image, five grid rotations and optimal z sectioning parameters were used. For each immunostained protein, all images were acquired with identical laser power and exposure time. After image acquisition, SIM images were reconstructed and subjected to deconvolution using default SIM processing parameters with Zeiss Zen Black 2.3 SP1 software. Automated Nup spot and volume analysis was conducted as previously described (8, 44) using Imaris version 9.2.0 (Bitplane) and the three-dimensional (3D) suite plugin in Fiji version 1.52p. Nup spots were counted using automated spot detection. A Bayesian classifier taking into account volume, average intensity, and contrast features was applied to detect and segment individual spots. The total number of Nup spots was determined using a 3D rendering of segmented SIM images comprising the entire depth of each nucleus. When individual Nup spots could not be resolved due to limits of resolution of immunofluorescent SIM, the percent total nuclear volume occupied by the Nup was calculated. To calculate total nuclear volume, X and Y axis length was measured in the center z slice for each nucleus, and Z axis length was estimated from the total z depth of acquired images. To calculate Nup volume, image

stacks were processed with automatic thresholding and automatic thresholding the 3D suite plugin in Fiji was used to determine the volume of the region previously subjected to automatic thresholding for each nucleus. Representative images are presented as 3D maximum intensity projections generated in Zeiss Zen Black 2.3 SP1. Images were faux colored green for contrast and display.

Immunostaining and confocal imaging of iPSNs

On day 12 of differentiation, iPSNs were plated in 24-well optical bottom plates (Cellvis). At days 25, 32, or 46 of differentiation (see individual figure legends), iPSNs were fixed in 4% PFA for 15 min, washed with 1× PBS three times for 10 min, permeabilized with 1× PBST containing 0.3% Triton X-100 for 15 min, blocked in 10% normal goat serum diluted in 1× PBS for 1 hour, and incubated in primary antibody for 2 hours at room temperature (see table S2 for antibody information). iPSNs were then washed with 1× PBS three times for 10 min, incubated in secondary antibody (see table S2 for antibody information) for 1 hour at room temperature, washed in 1× PBS two times for 10 min, incubated with Hoechst diluted 1:1000 in 1× PBS for 10 min, and washed in 1× PBS two times for 10 min. iPSNs were mounted using Prolong Gold Antifade Reagent with 4′,6-diamidino-2-phenylindole (DAPI). iPSNs were imaged using a Zeiss LSM 800 or Zeiss LSM 980 confocal microscope. All images were acquired using identical imaging parameters such as laser power and gain. Nuclear intensity and nuclear/cytoplasmic ratios were calculated with Fiji as previously described (8, 46). Images presented are maximum intensity projections generated in Zeiss Zen Blue 2.3.

Human tissue immunofluorescence

Nonneurological control and *C9orf72* patient postmortem paraffin-embedded motor and occipital cortex sections were obtained from D. Dickson (Mayo Clinic) and the Target ALS Human Postmortem Tissue Core (see table S3 for demographic information). Tissue sections were gradually rehydrated with xylene three times for 5 min, 100% ethanol two times for 5 min, 90% ethanol for 5 min, 70% ethanol for 5 min, and finally dH_2O three times for 5 min. Antigen retrieval was performed with Tissue-Tek antigen retrieval solution (IHC World) for 1 hour in a steamer. Slides were cooled for 10 min and washed three times for 5 min with dH_2O and three times for 5 min with 1× PBS and permeabilized with 0.4% Triton X-100 diluted in 1× PBS for 10 min on a shaker. Slides were subsequently washed three times for 5 min in 1× PBS blocked with DAKO protein-free serum block (DAKO) overnight at 4°C. Tissue sections were incubated with primary antibody (see table S2 for antibody information) diluted in DAKO antibody diluent reagent with background reducing components for a total of two overnights at 4°C. In between the two overnight incubations, slides were incubated in primary antibody at room temperature with gentle agitation for 10 hours. After primary antibody, tissue sections were washed three times for 5 min with 1× PBS and then incubated with secondary antibody (see table S2 for antibody information) diluted in DAKO antibody diluent with background reducing components (DAKO) at room temperature with gentle agitation for 1 hour. Slides were then washed three times for 5 min in 1× PBS, rinsed briefly with two to three drops of autofluorescence eliminator reagent (Millipore), and extensively washed five times for 5 min in 1× PBS to remove debris. Tissue sections were stained with Hoechst diluted 1:1000 in 1× PBS for 20 min and washed three

times for 5 min in 1× PBS. Slides were coverslipped using Prolong Gold Antifade Reagent with DAPI, and nuclei from Map2-positive Layer V neurons were imaged with a 20× objective and a Zeiss Axio Imager Z2 fluorescent microscope equipped with an Apotome2 module. All images were acquired using identical exposure times.

CHMP7 and TDP-43 nuclear/cytoplasmic ratios and nuclear intensities were quantified using Fiji. Briefly, in-focus neurons with visible nuclei were identified by positive Map2 and Hoechst signals. A small pixel box was used to measure fluorescent intensity in the CHMP7 or TDP-43 channel. Two integrated density measurements were taken from each cellular compartment (nucleus and cytoplasm), the average of which was used for subsequent analysis. Five background fluorescent intensity mean measurements were taken in areas devoid of cells, the average of which was used for analysis. Nuclear and cytoplasmic intensities were calculated as follows: Intensity = Integrated density – (Mean background intensity * Area measured within cell). The nuclear/cytoplasmic CHMP7 or TDP-43 ratio was calculated by dividing resulting nuclear intensity by cytoplasmic intensity for each cell. Nuclear intensities were obtained using the aforementioned calculation. Images are presented as default Apotome processed images generated in Zeiss Zen Blue 2.3.

Quantitative reverse transcription polymerase chain reaction

RNA from iPSNs was isolated with an RNeasy kit (QIAGEN) according to the manufacturer's protocol. RNA concentrations were determined with a NanoDrop 1000 spectrophotometer (Thermo Fisher Scientific). For CHMP7 ASO experiments, RNA was isolated on day 46 of differentiation after 3-week exposure to 5 μM CHMP7 ASO 2 or scrambled control ASO. For CHMP7 overexpression experiments, RNA was isolated on day 32 of differentiation (2 weeks after plasmid nucleofection). One microgram of RNA was used for complementary DNA (cDNA) synthesis with random hexamers and the SuperScript IV First-Strand cDNA Synthesis Kit (Thermo Fisher Scientific). qRT-PCRs were performed using TaqMan Gene Expression Master Mix (TaqMan), TaqMan Gene Expression Assays (see table S4), and an Applied Biosystems QuantStudio 3 Real-Time PCR Machine (Applied Biosystems). *STMN2* qRT-PCRs were conducted as previously described (34, 35) using SYBR Green Master Mix (Thermo Fisher Scientific). See table S4 for primer sequences. Glyceraldehyde-3-phosphate dehydrogenase (GAPDH) was used for normalization in all experiments.

Western blots

Nuclei lysates—After nuclei isolation, nuclei pellets were resuspended in 25 μl of RIPA buffer (Millipore) containing 1× protease inhibitor cocktail (Roche). Homogenates were spun at 12,000*g* for 15 min and 4°C to remove debris. The supernatant was transferred to a new Eppendorf tube, and protein concentrations were determined using a BCA protein estimation assay kit (Thermo Fisher Scientific). A 4× Laemmli buffer (Bio-Rad) was added to each sample to a final concentration of 1×, samples were heated at 100°C for 5 min, and 5 μg of protein was loaded into 4 to 20% acrylamide gels (Bio-Rad). Gels were run until the dye front reached the bottom. Protein was transferred onto a nitrocellulose membrane using the Trans-Blot Turbo Transfer System (Bio-Rad). Blots were blocked for 30 min with 5% nonfat milk in 1× TBST (tris-buffered saline with 0.1% Tween 20) and

incubated overnight at 4°C with primary antibody diluted in block (see table S2 for antibody information). The next day, blots were washed four times for 10 min with 1× TBST and probed with secondary antibody diluted in block (see table S2 for antibody information) for 1 hour at room temperature. Blots were subsequently washed four times for 10 min with 1× TBST, and an ECL substrate (Thermo Fisher Scientific, Millipore) was applied for 30 s. Chemiluminescent images were acquired with the GE Healthcare ImageQuant LAS 4000 system. To sequentially probe membranes without stripping, chemiluminescent signals were quenched by incubating blots in room temperature 30% H_2O_2 for 15 min (62). Analysis was conducted in Fiji. Lamin B1 was used for normalization.

iPSN lysates—On day 32 of differentiation, iPSNs were rinsed with ice-cold 1× Dulbecco's PBS (DPBS) with Ca^{2+} and Mg^{2+}. One milliliter of fresh 1× DPBS was added to each well, and iPSNs were harvested with a cell scraper and transferred to an Eppendorf tube. Cells were then pelleted at 2500 rpm at 4°C for 5 min. The supernatant was aspirated, and the resulting cell pellet was lysed in 50 μl of RIPA buffer containing 1× protease inhibitor cocktail. For ASO-treated iPSNs, cells were harvested and lysed on day 40 of differentiation. Western blots and analysis were performed as described above. GAPDH was used for normalization.

Plasmids and nucleofection for CHMP7 overexpression

The GFP-tagged CHMP7 plasmid was obtained from OriGene. To generate the CHMP7 NES mutant (CHMP7 NES*) plasmid, a singleamino acid substitution (amino acid 430, L to A) was created in the CHMP7 GFP plasmid (OriGene) using a Q5 site-directed mutagenesis kit (New England BioLabs). A GFP control plasmid was obtained from OriGene. See table S5 for plasmid information. On day 18 of differentiation, iPSNs were dissociated with accutase to assist with single-cell dissociation and nucleofected in suspension using the Lonza P3 Primary Cell 4D Nucleofector Kit (Lonza) and program DC104 on the Lonza nucleofection system. Each cuvette contained 5×10^6 iPSNs and 4 μg of plasmid DNA. After nucleofection, iPSNs were plated in Matrigel (Corning)–coated cell culture dishes according to Lonza protocol. Medium was exchanged on days 19 and 22 of differentiation. For overexpression of CHMP7 variants, downstream SIM experimentation was carried out on day 25 of differentiation, and TDP-43 localization and qRT-PCR analyses were carried out on day 32 of differentiation. For overexpression of LEMD2, SIM experiments were carried out on day 32 of differentiation.

Knockdown of POM121 and LEMD2 by Trim Away

Knockdown of endogenous POM121 and LEMD2 was carried out using a modified Trim Away protocol (23) as previously described (8). POM121 (Thermo Fisher Scientific) and LEMD2 (Thermo Fisher Scientific) antibodies were dialyzed in 1× PBS using the Slide-A-Lyzer MINI Dialysis Device, 20 K MWCO (Thermo Fisher Scientific). PBS was exchanged after 2 hours, and dialysis proceeded with gentle agitation at room temperature overnight. Dialyzed antibodies were concentrated with an Amicon Ulta-0.5 Centrifugal Filter Unit with Ultacell-100 membrane (Millipore). Resulting antibody concentration was calculated with a NanoDrop 1000 spectrophotometer (Thermo Fisher Scientific) as previously described (23). On day 18 of differentiation, iPSNs were dissociated with accutase. Suspension-based

nucleofection was carried out with the Lonza P3 Primary Cell 4D Nucleofector Kit (Lonza) and the program DC154. Each cuvette contained 5×10^6 iPSNs, 5 μg of antibody, and 4 μg of Trim21 GFP plasmid DNA (OriGene, see table S5). After nucleofection, iPSNs were replated in Matrigel (Corning)–coated cell culture dishes according to Lonza protocol and used for downstream analysis on day 20 of differentiation.

Glutamate toxicity

On day 12 of differentiation, iPSNs were plated in 24-well optical bottom plates (Cellvis) at a density of 250,000 neurons per well. Neurons were rinsed with 1× PBS and fed with fresh stage 3 media daily remove dead cells and debris until day 25 of differentiation. On day 25 of differentiation, ASO treatment was initiated as described above. Every 3 days, iPSNs were rinsed three times with 1× PBS and media and ASO were replaced. On day 40 of differentiation, iPSNs were washed with 1× PBS to remove any remaining debris and dead cells. Medium was replaced with artificial cerebrospinal fluid (Tocris) containing 0 or 10 μM glutamate (Sigma-Aldrich). iPSNs were incubated at 37°C with 5% CO_2 for 4 hours. After 3.5 hours, one drop of NucBlue Live ReadyProbes (Thermo Fisher Scientific) and 1 μM PI (Thermo Fisher Scientific) were added to each well and cells were returned to the incubator for 30 min. iPSNs were imaged in an environmentally controlled chamber with a Zeiss LSM 800 confocal microscope. Five images per well were acquired with a 10× objective. PI and DAPI spots were counted using Fiji.

Statistical analysis

All data analysis was conducted with Imaris or Fiji as described in each experimental section above and was either completely automated or blinded. All statistical analyses were performed using GraphPad Prism versions 8 and 9 (GraphPad). For imaging experiments where multiple cells or nuclei per iPSC line or patient were quantified, statistical analyses were performed such that the average of all nuclei or cells evaluated per iPSC line or patient represents $n = 1$, with total n per experiment and group as indicated in figure legends. All data were normally distributed. Student's t test, one-way analysis of variance (ANOVA) with Tukey's multiple comparison test, or two-way ANOVA with Tukey's multiple comparison test was used as described in figure legends. $^*P < 0.05$, $^{**}P < 0.01$, $^{***}P < 0.001$, and $^{****}P < 0.0001$. Violin plots are used to display the full spread and variability of large datasets (>10 data points). Center dotted line indicates median value. Two additional dotted lines indicate the 25th and 75th percentiles. For smaller datasets, bar graphs displaying individual data points are shown, where error bars represent ±SEM.

Supplementary Material

Refer to Web version on PubMed Central for supplementary material.

Acknowledgments:

We thank the ALS patients and their families for essential contributions to this research and the Target ALS Human Postmortem Tissue Core and Dennis Dickson (Mayo Clinic) for providing postmortem human tissue.

Funding:

This work was supported by funding from NIH grants P01NS099114, U54NS091046, and R01NS094239 to J.D.R. and R01NS122236 to J.D.R. and C.P.L.; Department of Defense, The Robert Packard Center for ALS Research Answer ALS Program, ALS Finding a Cure, ALS Association, Muscular Dystrophy Association, Virginia Gentleman Foundation, F Prime, and the Chan Zuckerberg Initiative to J.D.R.; and the ALSA Milton Safenowitz Postdoctoral Fellowship and NIH grant K99NS123242 to A.N.C.

Competing interests:

A.N.C. and J.D.R. have submitted a patent application (U.S. Patent Application Serial No. 63/111,882) regarding methods for inhibiting CHMP7 expression in neuronal cells for the treatment of neurodegenerative disorders. J.D.R. is a consultant for Expansion Therapeutics and has received research grants from Calico and GlaxoSmithKline.

REFERENCES AND NOTES

1. Ling SC, Polymenidou M, Cleveland DW, Converging mechanisms in ALS and FTD: Disrupted RNA and protein homeostasis. Neuron 79, 416–438 (2013). [PubMed: 23931993]
2. Taylor JP, Brown RH Jr., Cleveland DW, Decoding ALS: From genes to mechanism. Nature 539, 197–206 (2016). [PubMed: 27830784]
3. Kim G, Gautier O, Tassoni-Tsuchida E, Ma XR, Gitler AD, ALS genetics: Gains, losses, and implications for future therapies. Neuron 108, 822–842 (2020). [PubMed: 32931756]
4. Sances S, Bruijn LI, Chandran S, Eggan K, Ho R, Klim JR, Livesey MR, Lowry E, Macklis JD, Rushton D, Sadegh C, Sareen D, Wichterle H, Zhang S-C, Svendsen CN, Modeling ALS with motor neurons derived from human induced pluripotent stem cells. Nat. Neurosci 19, 542–553 (2016). [PubMed: 27021939]
5. Zhang X, Hu D, Shang Y, Qi X, Using induced pluripotent stem cell neuronal models to study neurodegenerative diseases. Biochim. Biophys. Acta Mol. Basis Dis 1866, 165431 (2019). [PubMed: 30898538]
6. Donnelly CJ, Zhang P-W, Pham JT, Haeusler AR, Mistry NA, Vidensky S, Daley EL, Poth EM, Hoover B, Fines DM, Maragakis N, Tienari PJ, Petrucelli L, Traynor BJ, Wang J, Rigo F, Bennett CF, Blackshaw S, Sattler R, Rothstein JD, RNA toxicity from the ALS/FTD C9ORF72 expansion is mitigated by antisense intervention. Neuron 80, 415–428 (2013). [PubMed: 24139042]
7. Gendron TF, Chew J, Stankowski JN, Hayes LR, Zhang Y-J, Prudencio M, Carlomagno Y, Daughrity LM, Jansen-West K, Perkerson EA, O'Raw A, Cook C, Pregent L, Belzil V, van Blitterswijk M, Tabassian LJ, Lee CW, Yue M, Tong J, Song Y, Castanedes-Casey M, Rousseau L, Phillips V, Dickson DW, Rademakers R, Fryer JD, Rush BK, Pedraza O, Caputo AM, Desaro P, Palmucci C, Robertson A, Heckman MG, Diehl NN, Wiggs E, Tierney M, Braun L, Farren J, Lacomis D, Ladha S, Fournier CN, McCluskey LF, Elman LB, Toledo JB, McBride JD, Tiloca C, Morelli C, Poletti B, Solca F, Prelle A, Wuu J, Jockel-Balsarotti J, Rigo F, Ambrose C, Datta A, Yang W, Raitcheva D, Antognetti G, McCampbell A, van Swieten JC, Miller BL, Boxer AL, Brown RH, Bowser R, Miller TM, Trojanowski JQ, Grossman M, Berry JD, Hu WT, Ratti A, Traynor BJ, Disney MD, Benatar M, Silani V, Glass JD, Floeter MK, Rothstein JD, Boylan KB, Petrucelli L, Poly(GP) proteins are a useful pharmacodynamic marker forC9ORF72-associated amyotrophic lateral sclerosis. Sci. Transl. Med 9, eaai7866 (2017). [PubMed: 28356511]
8. Coyne AN, Zaepfel BL, Hayes L, Fitchman B, Salzberg Y, Luo E-C, Bowen K, Trost H, Aigner S, Rigo F, Yeo GW, Harel A, Svendsen CN, Sareen D, Rothstein JD, G4C2 repeat RNA initiates a POM121-mediated reduction in specific nucleoporins in C9orf72 ALS/FTD. Neuron 107, 1124–1140.e11 (2020). [PubMed: 32673563]
9. Beck M, Hurt E, The nuclear pore complex: Understanding its function through structural insight. Nat. Rev. Mol. Cell Biol 18, 73–89 (2017). [PubMed: 27999437]
10. Lin DH, Hoelz A, The structure of the nuclear pore complex (an update). Annu. Rev. Biochem 88, 725–783 (2019). [PubMed: 30883195]
11. Raices M, D'Angelo MA, Nuclear pore complex composition: A new regulator of tissue-specific and developmental functions. Nat. Rev. Mol. Cell Biol 13, 687–699 (2012). [PubMed: 23090414]
12. Raices M, D'Angelo MA, Nuclear pore complexes and regulation of gene expression. Curr. Opin. Cell Biol 46, 26–32 (2017). [PubMed: 28088069]

13. Webster BM, Colombi P, Jager J, Lusk CP, Surveillance of nuclear pore complex assembly by ESCRT-III/Vps4. Cell 159, 388–401 (2014). [PubMed: 25303532]
14. Thaller DJ, Allegretti M, Borah S, Ronchi P, Beck M, Lusk CP, An ESCRT-LEM protein surveillance system is poised to directly monitor the nuclear envelope and nuclear transport system. eLife 8, e45284 (2019). [PubMed: 30942170]
15. Webster BM, Thaller DJ, Jäger J, Ochmann SE, Borah S, Lusk CP, Chm7 and Heh1 collaborate to link nuclear pore complex quality control with nuclear envelope sealing. EMBO J. 35, 2447–2467 (2016). [PubMed: 27733427]
16. Toyama BH, Drigo RAE, Lev-Ram V, Ramachandra R, Deerinck TJ, Lechene C, Ellisman MH, Hetzer MW, Visualization of long-lived proteins reveals age mosaicism within nuclei of postmitotic cells. J. Cell Biol 218, 433–444 (2018). [PubMed: 30552100]
17. Lee CW, Wilfling F, Ronchi P, Allegretti M, Mosalaganti S, Jentsch S, Beck M, Pfander B, Selective autophagy degrades nuclear pore complexes. Nat. Cell Biol 22, 159–166 (2020). [PubMed: 32029894]
18. Tomioka Y, Kotani T, Kirisako H, Oikawa Y, Kimura Y, Hirano H, Ohsumi Y, Nakatogawa H, TORC1 inactivation stimulates autophagy of nucleoporin and nuclear pore complexes. J. Cell Biol 219, e201910063 (2020). [PubMed: 32453403]
19. Lusk CP, Ader NR, CHMPions of repair: Emerging perspectives on sensing and repairing the nuclear envelope barrier. Curr. Opin. Cell Biol 64, 25–33 (2020). [PubMed: 32105978]
20. Robberecht W, Philips T, The changing scene of amyotrophic lateral sclerosis. Nat. Rev. Neurosci 14, 248–264 (2013). [PubMed: 23463272]
21. Maglione M, Sigrist SJ, Seeing the forest tree by tree: Super-resolution light microscopy meets the neurosciences. Nat. Neurosci 16, 790–797 (2013). [PubMed: 23799471]
22. Schermelleh L, Carlton PM, Haase S, Shao L, Winoto L, Kner P, Burke B, Cardoso MC, Agard DA, Gustafsson MGL, Leonhardt H, Sedat JW, Subdiffraction multicolor imaging of the nuclear periphery with 3D structured illumination microscopy. Science 320, 1332–1336 (2008). [PubMed: 18535242]
23. Clift D, McEwan WA, Labzin LI, Konieczny V, Mogessie B, James LC, Schuh M, A method for the acute and rapid degradation of endogenous proteins. Cell 171, 1692–1706.e18 (2017). [PubMed: 29153837]
24. Boeynaems S, Bogaert E, Van Damme P, Van Den Bosch L, Inside out: The role of nucleocytoplasmic transport in ALS and FTLD. Acta Neuropathol. 132, 159–173 (2016). [PubMed: 27271576]
25. Hutten S, Dormann D, Nucleocytoplasmic transport defects in neurodegeneration-Cause or consequence? Semin. Cell Dev. Biol. 99, 151–162 (2019). [PubMed: 31152789]
26. Jovicic A, Paul III JW, Gitler AD, Nuclear transport dysfunction: A common theme in amyotrophic lateral sclerosis and frontotemporal dementia. J. Neurochem 138 (Suppl 1), 134–144 (2016). [PubMed: 27087014]
27. Kim HJ, Taylor JP, Lost in transportation: Nucleocytoplasmic transport defects in ALS and other neurodegenerative diseases. Neuron 96, 285–297 (2017). [PubMed: 29024655]
28. Vietri M, Schultz SW, Bellanger A, Jones CM, Petersen LI, Raiborg C, Skarpen E, Pedurupillay CRJ, Kjos I, Kip E, Timmer R, Jain A, Collas P, Knorr RL, Grellscheid SN, Kusumaatmaja H, Brech A, Micci F, Stenmark H, Campsteijn C, Unrestrained ESCRT-III drives micronuclear catastrophe and chromosome fragmentation. Nat. Cell Biol 22, 856–867 (2020). [PubMed: 32601372]
29. Gu M, LaJoie D, Chen O-S, von Appen A, Ladinsky MS, Redd MJ, Nikolova L, Bjorkman PJ, Sundquist WI, Ullman KS, Frost A, LEM2 recruits CHMP7 for ESCRT-mediated nuclear envelope closure in fission yeast and human cells. Proc. Natl. Acad. Sci. U.S.A 114, E2166–E2175 (2017). [PubMed: 28242692]
30. Suk TR, Rousseaux MWC, The role of TDP-43 mislocalization in amyotrophic lateral sclerosis. Mol. Neurodegener 15, 45 (2020). [PubMed: 32799899]
31. Vatsavayai SC, Yoon SJ, Gardner RC, Gendron TF, Vargas JNS, Trujillo A, Pribadi M, Phillips JJ, Gaus SE, Hixson JD, Garcia PA, Rabinovici GD, Coppola G, Geschwind DH, Petrucelli L,

Miller BL, Seeley WW, Timing and significance of pathological features in C9orf72 expansion-associated frontotemporal dementia. Brain J. Neurol 139, 3202–3216 (2016).

32. Gao J, Wang L, Huntley ML, Perry G, Wang X, Pathomechanisms of TDP-43 in neurodegeneration. J. Neurochem 146, 7–20 (2018).
33. Coyne AN, Zaepfel BL, Zarnescu DC, Failure to deliver and translate-new insights into RNA dysregulation in ALS. Front. Cell. Neurosci 11, 243 (2017). [PubMed: 28860970]
34. Melamed Z, López-Erauskin J, Baughn MW, Zhang O, Drenner K, Sun Y, Freyermuth F, Mahon MAM, Beccari MS, Artates JW, Ohkubo T, Rodriguez M, Lin N, Wu D, Bennett CF, Rigo F, Cruz SD, Ravits J, Lagier-Tourenne C, Cleveland DW, Premature polyadenylation-mediated loss of stathmin-2 is a hallmark of TDP-43-dependent neurodegeneration. Nat. Neurosci 22, 180–190 (2019). [PubMed: 30643298]
35. Prudencio M, Humphrey J, Pickles S, Brown AL, Hill SE, Kachergus JM, Shi J, Heckman MG, Spiegel MR, Cook C, Song Y, Yue M, Daughrity LM, Carlomagno Y, Jansen-West K, de Castro CF, DeTure M, Koga S, Wang YC, Sivakumar P, Bodo C, Candalija A, Talbot K, Selvaraj BT, Burr K, Chandran S, Newcombe J, Lashley T, Hubbard I, Catalano D, Kim D, Propp N, Fennessey S;NYGC ALS Consortium, Fagegaltier D, Phatnani H, Secrier M, Fisher EM, Oskarsson B, van Blitterswijk M, Rademakers R, Graff-Radford NR, Boeve BF, Knopman DS, Petersen RC, Josephs KA, Thompson EA, Raj T, Ward M, Dickson DW, Gendron TF, Fratta P, Petrucelli L, Truncated stathmin-2 is a marker of TDP-43 pathology in frontotemporal dementia. J. Clin. Invest 130, 6080–6092 (2020). [PubMed: 32790644]
36. Klim JR, Williams LA, Limone F, Guerra San Juan I, Davis-Dusenbery BN, Mordes DA, Burberry A, Steinbaugh MJ, Gamage KK, Kirchner R, Moccia R, Cassel SH, Chen K, Wainger BJ, Woolf CJ, Eggan K, ALS-implicated protein TDP-43 sustains levels of STMN2, a mediator of motor neuron growth and repair. Nat. Neurosci 22, 167–179 (2019). [PubMed: 30643292]
37. DeTure MA, Dickson DW, The neuropathological diagnosis of Alzheimer's disease. Mol. Neurodegener 14, 32 (2019). [PubMed: 31375134]
38. Johnson VE, Stewart W, Trojanowski JQ, Smith DH, Acute and chronically increased immunoreactivity to phosphorylation-independent but not pathological TDP-43 after a single traumatic brain injury in humans. Acta Neuropathol 122, 715–726 (2011). [PubMed: 22101322]
39. Thammisetty SS, Pedragosa J, Weng YC, Calon F, Planas A, Kriz J, Age-related deregulation of TDP-43 after stroke enhances NF-κB-mediated inflammation and neuronal damage. J. Neuroinflammation 15, 312 (2018). [PubMed: 30413172]
40. DeVos SL, Miller TM, Antisense oligonucleotides: Treating neurodegeneration at the level of RNA. Neurotherapeutics 10, 486–497 (2013). [PubMed: 23686823]
41. Schoch KM, Miller TM, Antisense oligonucleotides: Translation from mouse models to human neurodegenerative diseases. Neuron 94, 1056–1070 (2017). [PubMed: 28641106]
42. Melchior F, Ran GTPase cycle: One mechanism—Two functions. Curr. Biol 11, R257–R260 (2001). [PubMed: 11413013]
43. Chou CC, Zhang Y, Umoh ME, Vaughan SW, Lorenzini I, Liu F, Sayegh M, Donlin-Asp PG, Chen YH, Duong DM, Seyfried NT, Powers MA, Kukar T, Hales CM, Gearing M, Cairns NJ, Boylan KB, Dickson DW, Rademakers R, Zhang Y-J, Petrucelli L, Sattler R, Zarnescu DC, Glass JD, Rossoll W, TDP-43 pathology disrupts nuclear pore complexes and nucleocytoplasmic transport in ALS/FTD. Nat. Neurosci 21,228–239 (2018). [PubMed: 29311743]
44. Eftekharzadeh B, Daigle JG, Kapinos LE, Coyne A, Schiantarelli J, Carlomagno Y, Cook C, Miller SJ, Dujardin S, Amaral AS, Grima JC, Bennett RE, Tepper K, De Ture M, Vanderburg CR, Corjuc BT, De Vos SL, Gonzalez JA, Chew J, Vidensky S, Gage FH, Mertens J, Troncoso J, Mandelkow E, Salvatella X, Lim RYH, Petrucelli L, Wegmann S, Rothstein JD, Hyman BT, Tau protein disrupts nucleocytoplasmic transport in Alzheimer's disease. Neuron 99, 925–940.e7 (2018). [PubMed: 30189209]
45. Grima JC, Daigle JG, Arbez N, Cunningham KC, Zhang K, Ochaba J, Geater C, Morozko E, Stocksdale J, Glatzer JC, Pham JT, Ahmed I, Peng Q, Wadhwa H, Pletnikova O, Troncoso JC, Duan W, Snyder SH, Ranum LPW, Thompson LM, Lloyd TE, Ross CA, Rothstein JD, Mutant huntingtin disrupts the nuclear pore complex. Neuron 94, 93–107.e6 (2017). [PubMed: 28384479]
46. Zhang K, Donnelly CJ, Haeusler AR, Grima JC, Machamer JB, Steinwald P, Daley EL, Miller SJ, Cunningham KM, Vidensky S, Gupta S, Thomas MA, Hong I, Chiu SL, Huganir RL, Ostrow LW,

Matunis MJ, Wang J, Sattler R, Lloyd TE, Rothstein JD, The C9orf72 repeat expansion disrupts nucleocytoplasmic transport. Nature 525, 56–61 (2015). [PubMed: 26308891]

47. Chew J, Cook C, Gendron TF, Jansen-West K, del Rosso G, Daughrity LM, Castanedes-Casey M, Kurti A, Stankowski JN, Disney MD, Rothstein JD, Dickson DW, Fryer JD, Zhang Y-J, Petrucelli L, Aberrant deposition of stress granule-resident proteins linked to C9orf72-associated TDP-43 proteinopathy. Mol. Neurodegener 14, 9 (2019). [PubMed: 30767771]
48. Zhang YJ, Gendron TF, Ebbert MTW, O'Raw AD, Yue M, Jansen-West K, Zhang X, Prudencio M, Chew J, Cook CN, Daughrity LM, Tong J, Song Y, Pickles SR, Castanedes-Casey M, Kurti A, Rademakers R, Oskarsson B, Dickson DW, Hu W, Gitler AD, Fryer JD, Petrucelli L, Poly(GR) impairs protein translation and stress granule dynamics in C9orf72-associated frontotemporal dementia and amyotrophic lateral sclerosis. Nat. Med 24, 1136–1142 (2018). [PubMed: 29942091]
49. Zhang YJ, Gendron TF, Grima JC, Sasaguri H, Jansen-West K, Xu Y-F, Katzman RB, Gass J, Murray ME, Shinohara M, Lin W-L, Garrett A, Stankowski JN, Daughrity L, Tong J, Perkerson EA, Yue M, Chew J, Castanedes-Casey M, Kurti A, Wang ZS, Liesinger AM, Baker JD, Jiang J, Lagier-Tourenne C, Edbauer D, Cleveland DW, Rademakers R, Boylan KB, Bu G, Link CD, Dickey CA, Rothstein JD, Dickson DW, Fryer JD, Petrucelli L, C9ORF72 poly(GA) aggregates sequester and impair HR23 and nucleocytoplasmic transport proteins. Nat. Neurosci 19, 668–677 (2016). [PubMed: 26998601]
50. Zhang Y-J, Guo L, Gonzales PK, Gendron TF, Wu Y, Jansen-West K, O'Raw AD, Pickles SR, Prudencio M, Carlomagno Y, Gachechiladze MA, Ludwig C, Tian R, Chew J, De Ture M, Lin W-L, Tong J, Daughrity LM, Yue M, Song Y, Andersen JW, Castanedes-Casey M, Kurti A, Datta A, Antognetti G, Campbell AM, Rademakers R, Oskarsson B, Dickson DW, Kampmann M, Ward ME, Fryer JD, Link CD, Shorter J, Petrucelli L, Heterochromatin anomalies and double-stranded RNA accumulation underlie C9orf72 poly(PR) toxicity. Science 363, eaav2606 (2019). [PubMed: 30765536]
51. Thevathasan JV, Kahnwald M, Cieśliński K, Hoess P, Peneti SK, Reitberger M, Heid D, Kasuba KC, Hoerner SJ, Li Y, Wu Y-L, Mund M, Matti U, Pereira PM, Henriques R, Nijmeijer B, Kueblbeck M, Sabinina VJ, Ellenberg J, Ries J, Nuclear pores as versatile reference standards for quantitative superresolution microscopy. Nat. Methods 16, 1045–1053 (2019). [PubMed: 31562488]
52. McCullough J, Frost A, Sundquist WI, Structures, functions, and dynamics of ESCRT-III/Vps4 membrane remodeling and fission complexes. Annu. Rev. Cell Dev. Biol 34, 85–109 (2018). [PubMed: 30095293]
53. Vietri M, Radulovic M, Stenmark H, The many functions of ESCRTs. Nat. Rev. Mol. Cell Biol 21,25–42 (2019). [PubMed: 31705132]
54. Skibinski G, Parkinson NJ, Brown JM, Chakrabarti L, Lloyd SL, Hummerich H, Nielsen JE, Hodges JR, Spillantini MG, Thusgaard T, Brandner S, Brun A, Rossor MN, Gade A, Johannsen P, Sørensen SA, Gydesen S, Fisher EM-C, Collinge J, Mutations in the endosomal ESCRTIII-complex subunit CHMP2B in frontotemporal dementia. Nat. Genet 37, 806–808 (2005). [PubMed: 16041373]
55. Chang XL, Tan MS, Tan L, Yu JT, The role of TDP-43 in Alzheimer's disease. Mol. Neurobiol 53, 3349–3359 (2016). [PubMed: 26081142]
56. Neumann M, Sampathu DM, Kwong LK, Truax AC, Micsenyi MC, Chou TT, Bruce J, Schuck T, Grossman M, Clark CM, Mc Cluskey LF, Miller BL, Masliah E, Mackenzie IR, Feldman H, Feiden W, Kretzschmar HA, Trojanowski JQ, Lee VM-Y, Ubiquitinated TDP-43 in frontotemporal lobar degeneration and amyotrophic lateral sclerosis. Science 314, 130–133 (2006). [PubMed: 17023659]
57. Josephs KA, Whitwell JL, Weigand SD, Murray ME, Tosakulwong N, Liesinger AM, Petrucelli L, Senjem ML, Knopman DS, Boeve BF, Ivnik RJ, Smith GE, Jack CR Jr., Parisi JE, Petersen RC, Dickson DW, TDP-43 is a key player in the clinical features associated with Alzheimer's disease. Acta Neuropathol 127, 811–824 (2014). [PubMed: 24659241]
58. Robinson JL, Lee EB, Xie SX, Rennert L, Suh E-R, Bredenberg C, Caswell C, van Deerlin VM, Yan N, Yousef A, Hurtig HI, Siderowf A, Grossman M, McMillan CT, Miller B, Duda JE, Irwin DJ, Wolk D, Elman L, McCluskey L, Chen-Plotkin A, Weintraub D, Arnold SE, Brettschneider J,

Lee VM-Y, Trojanowski JQ, Neurodegenerative disease concomitant proteinopathies are prevalent, age-related and APOE4-associated. Brain J. Neurol 141,2181–2193 (2018).

59. Vossel KA, Bien-Ly N, Bernardo A, Rascovsky K, Karydas A, Rabinovici GD, Sidhu M, Huang EJ, Miller BL, Huang Y, Seeley WW, ApoE and TDP-43 neuropathology in two siblings with familial FTLD-motor neuron disease. Neurocase 19, 295–301 (2013). [PubMed: 22512241]
60. Wennberg AM, Tosakulwong N, Lesnick TG, Murray ME, Whitwell JL, Liesinger AM, Petrucelli L, Boeve BF, Parisi JE, Knopman DS, Petersen RC, Dickson DW, Josephs KA, Association of apolipoprotein E ε4 with transactive response DNA-binding protein 43. JAMA Neurol. 75, 1347–1354 (2018). [PubMed: 30422173]
61. Yang HS, Yu L, White CC, Chibnik LB, Chhatwal JP, Sperling RA, Bennett DA, Schneider JA, de Jager PL, Evaluation of TDP-43 proteinopathy and hippocampal sclerosis in relation to APOE ε4 haplotype status: A community-based cohort study. Lancet Neurol. 17, 773–781 (2018). [PubMed: 30093249]
62. Sennepin AD, Charpentier S, Normand T, Sarré C, Legrand A, Mollet LM, Multiple reprobing of Western blots after inactivation of peroxidase activity by its substrate, hydrogen peroxide. Anal. Biochem 393, 129–131 (2009). [PubMed: 19523435]

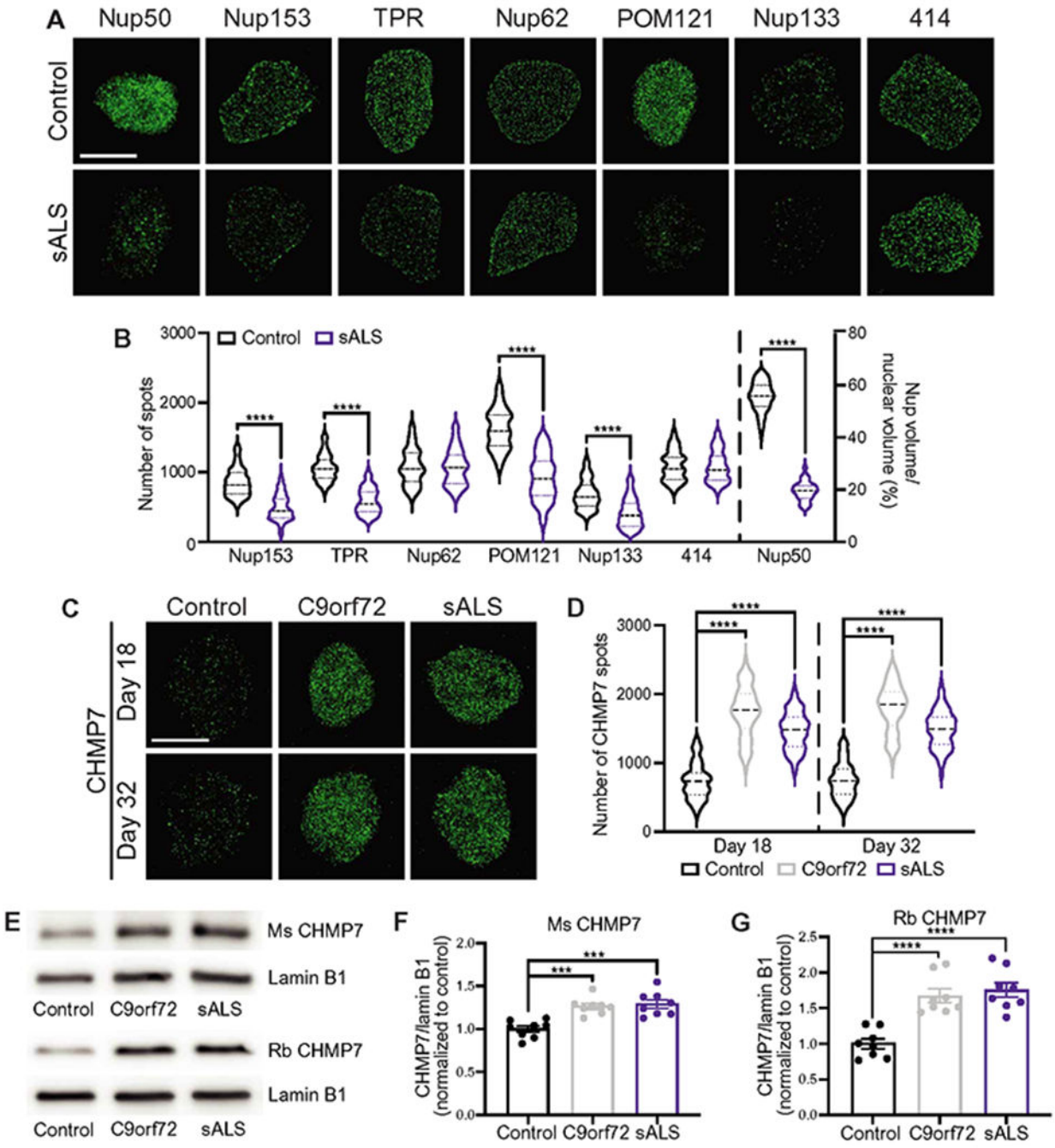

Fig. 1. Increased nuclear expression of CHMP7 correlates with reduction in specific Nups in *C9orf72* and sALS iPSN nuclei.

(**A**) Maximum intensity projections from SIM imaging of Nups in nuclei isolated from control and sALS iPSNs at day 32 of differentiation. Genotype as indicated on left, antibody as indicated on top. (**B**) Quantification of Nup spots. $n = 10$ control and 17 sALS iPSC lines, 50 $NeuN^+$ nuclei per line. Student's t test was used to calculate statistical significance. **** $P < 0.0001$. (**C**) Maximum intensity projections from SIM imaging of CHMP7 in nuclei isolated from control, *C9orf72*, and sALS iPSNs. Time point as indicated on left, genotype

as indicated on top. (**D**) Quantification of CHMP7 spots. $n = 10$ control, 8 *C9orf72*, and 17 sALS iPSC lines, 50 $NeuN^+$ nuclei per line. One-way ANOVA with Tukey's multiple comparison test was used to calculate statistical significance. ****$P < 0.0001$. (**E** to **G**) Western blot (E) and quantification (F and G) for CHMP7 expression in nuclei isolated from day 18 control, *C9orf72*, and sALS iPSNs. Antibodies as indicated on right, genotype as indicated on bottom. Note: Two independent CHMP7 antibodies were used. Lamin B1 was used as a loading control. $n = 8$ control, 8 *C9orf72*, and 8 sALS iPSC lines. One-way ANOVA with Tukey's multiple comparison test was used to calculate statistical significance. ***$P < 0.001$ and ****$P < 0.0001$. Scale bar, 5 μm.

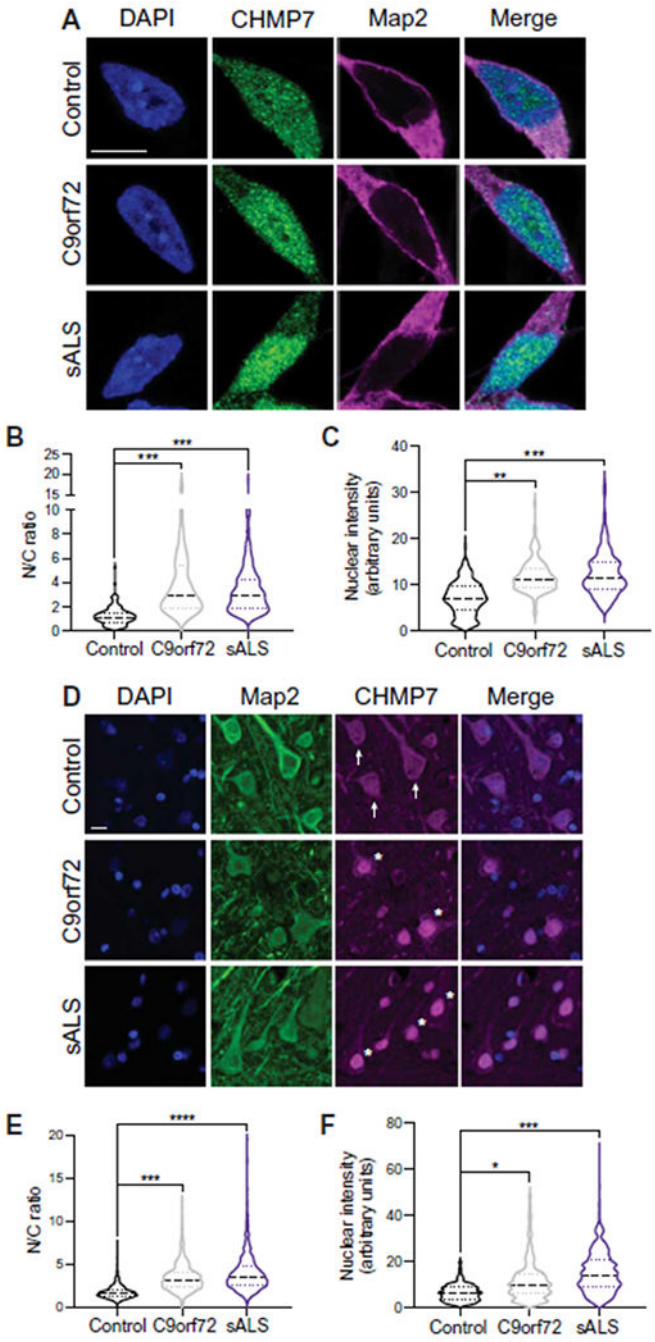

Fig. 2. The nuclear localization of CHMP7 is increased in *C9orf72* and sALS iPSNs and postmortem patient motor cortex.

(**A**) Immunostaining and confocal imaging for CHMP7 in iPSNs at day 25 of differentiation. Genotype as indicated on left, antibody as indicated on top. (**B** and **C**) Quantification of nuclear/cytoplasmic (N/C) ratio (B) and nuclear intensity (C) of CHMP7 immunostaining. n = 7 control, 5 *C9orf72*, and 7 sALS iPSC lines, at least 50 Map2$^+$ neurons per line. One-way ANOVA with Tukey's multiple comparison test was used to calculate statistical significance. ** $P < 0.01$ and *** $P < 0.001$. (**D**) Immunostaining for CHMP7 in paraffin-embedded

postmortem motor cortex. Genotype as indicated on left, antibody as indicated on top. Arrows indicate cytoplasmic CHMP7 immunostaining. Asterisks indicate nuclear CHMP7 immunostaining. (**E** and **F**) Quantification of nuclear/cytoplasmic ratio (E) and nuclear intensity (F) of CHMP7 immunostaining. $n = 13$ control, 17 *C9orf72*, and 30 sALS cases, at least 100 $Map2^+$ cells per case. One-way ANOVA with Tukey's multiple comparison test was used to calculate statistical significance. $*P < 0.05$, $***P < 0.001$, and $****P < 0.0001$. Scale bars, 10 μm.

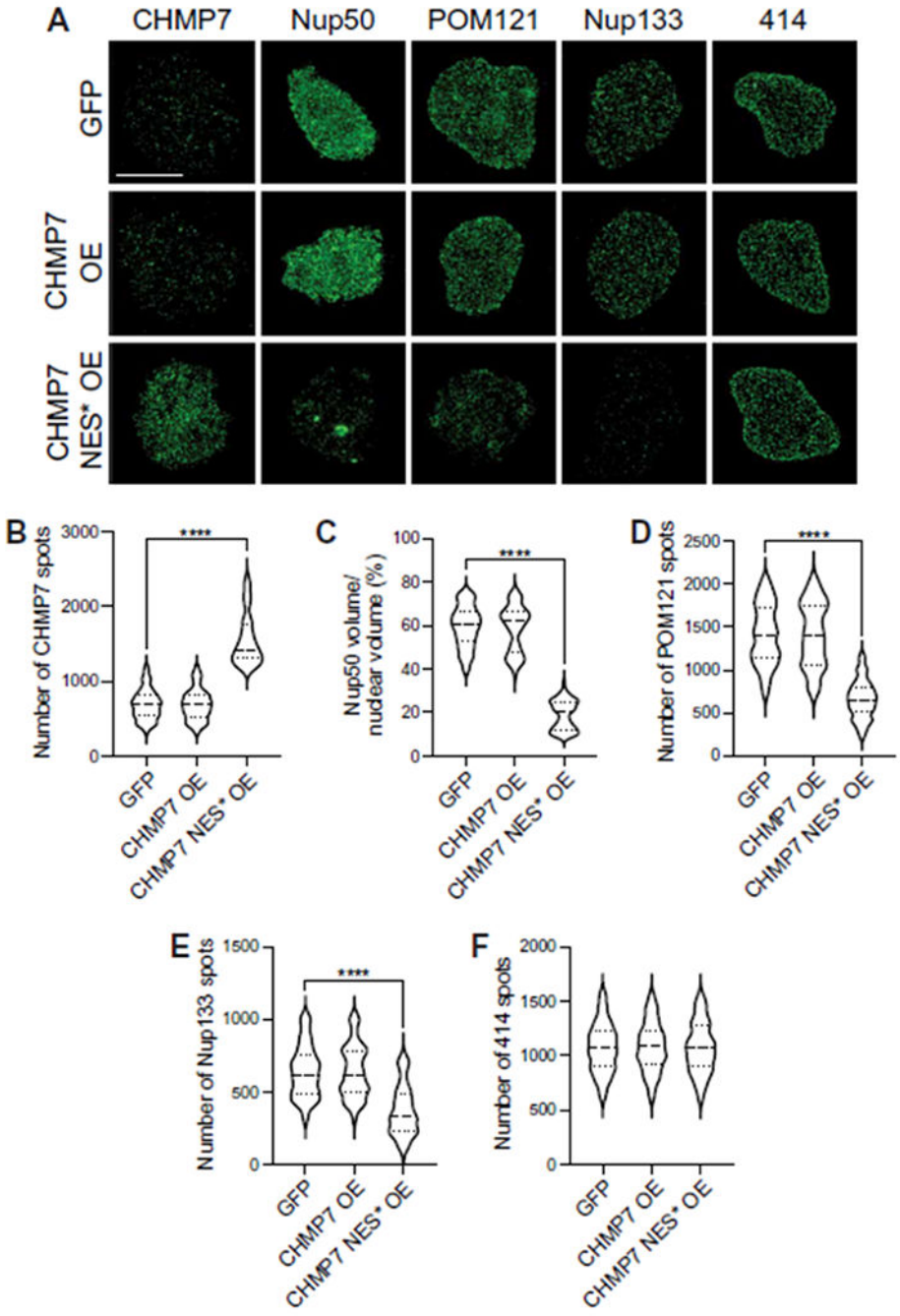

Fig. 3. Inhibition of CHMP7 nuclear export in wild-type iPSNs recapitulates disease-associated Nup alterations.

(**A**) Maximum intensity projections from SIM imaging of nuclei isolated from control iPSNs on day 25 of differentiation after 1 week of GFP-tagged CHMP7 variant overexpression (OE). Overexpression as indicated on left, antibodies as indicated on top. (**B** to **F**) Quantification of CHMP7 spots (B), Nup50 volume (C), and POM121 (D), Nup133 (E), and 414 (F) spots. $n = 4$ control iPSC lines, 50 GFP^+ nuclei per line/overexpression. One-way

ANOVA with Tukey's multiple comparison test was used to calculate statistical significance. **** $P < 0.0001$. Scale bar, 5 μm.

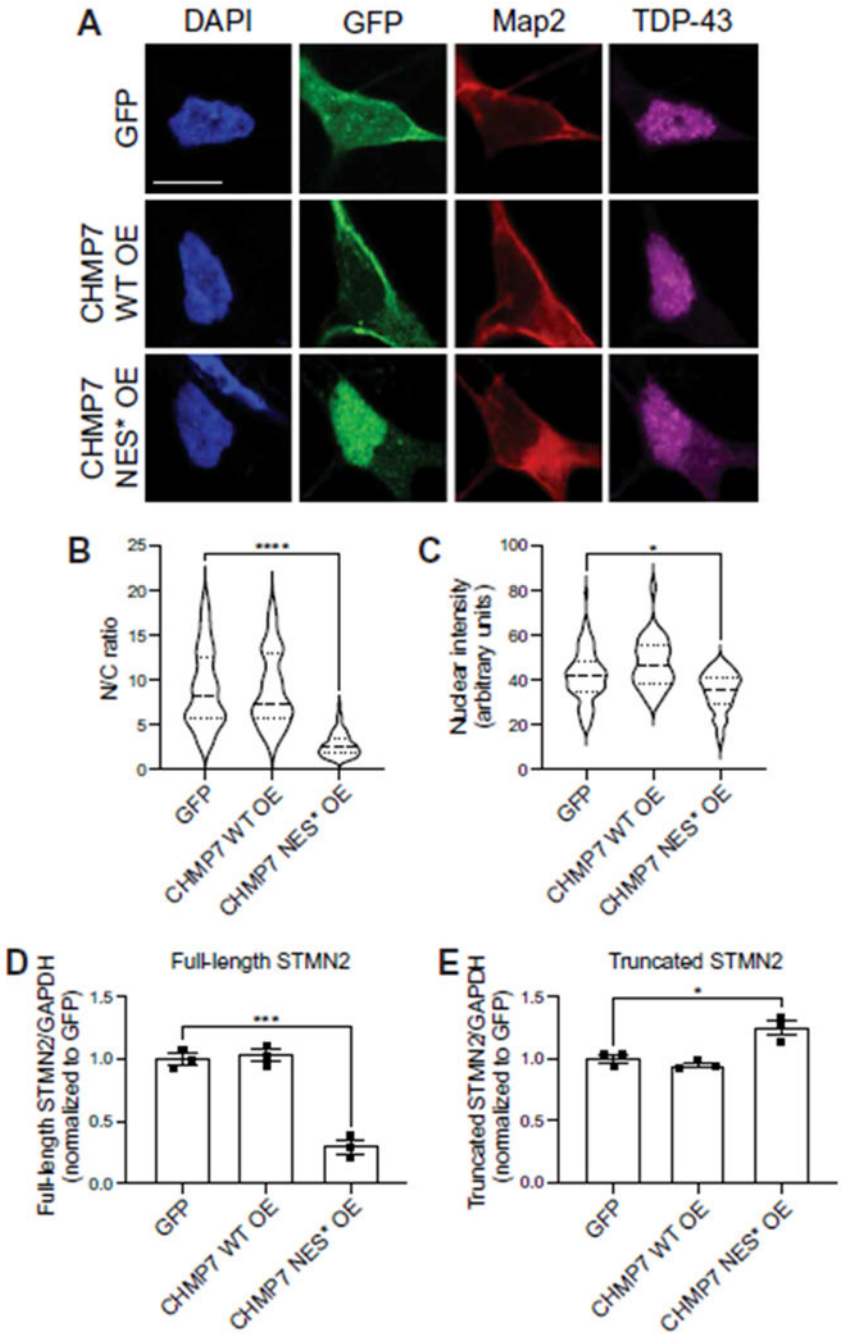

Fig. 4. Inhibition of CHMP7 nuclear export affects TDP-43 localization and function.

(**A**) Immunostaining and confocal imaging for TDP-43 in control iPSNs on day 32 of differentiation after 2 weeks of GFP-tagged CHMP7 variant overexpression. Overexpression as indicated on left, antibodies as indicated on top. WT, wild type. (**B** and **C**) Quantification of nuclear/cytoplasmic ratio (B) and nuclear intensity (C) of TDP-43 immunostaining. $n = 3$ control iPSC lines, at least 50 $Map2^+$ and GFP^+ neurons per line/overexpression. One-way ANOVA with Tukey's multiple comparison test was used to calculate statistical significance. $*P < 0.05$ and $****P < 0.0001$. (**D** and **E**) qRT-PCR for full-length (D) and truncated (E)

STMN2 mRNA in control iPSNs on day 32 of differentiation after 2 weeks of GFP-tagged CHMP7 variant overexpression. GAPDH was used for normalization. One-way ANOVA with Tukey's multiple comparison test was used to calculate statistical significance. $*P < 0.05$ and $***P < 0.001$. Scale bar, 10 μm.

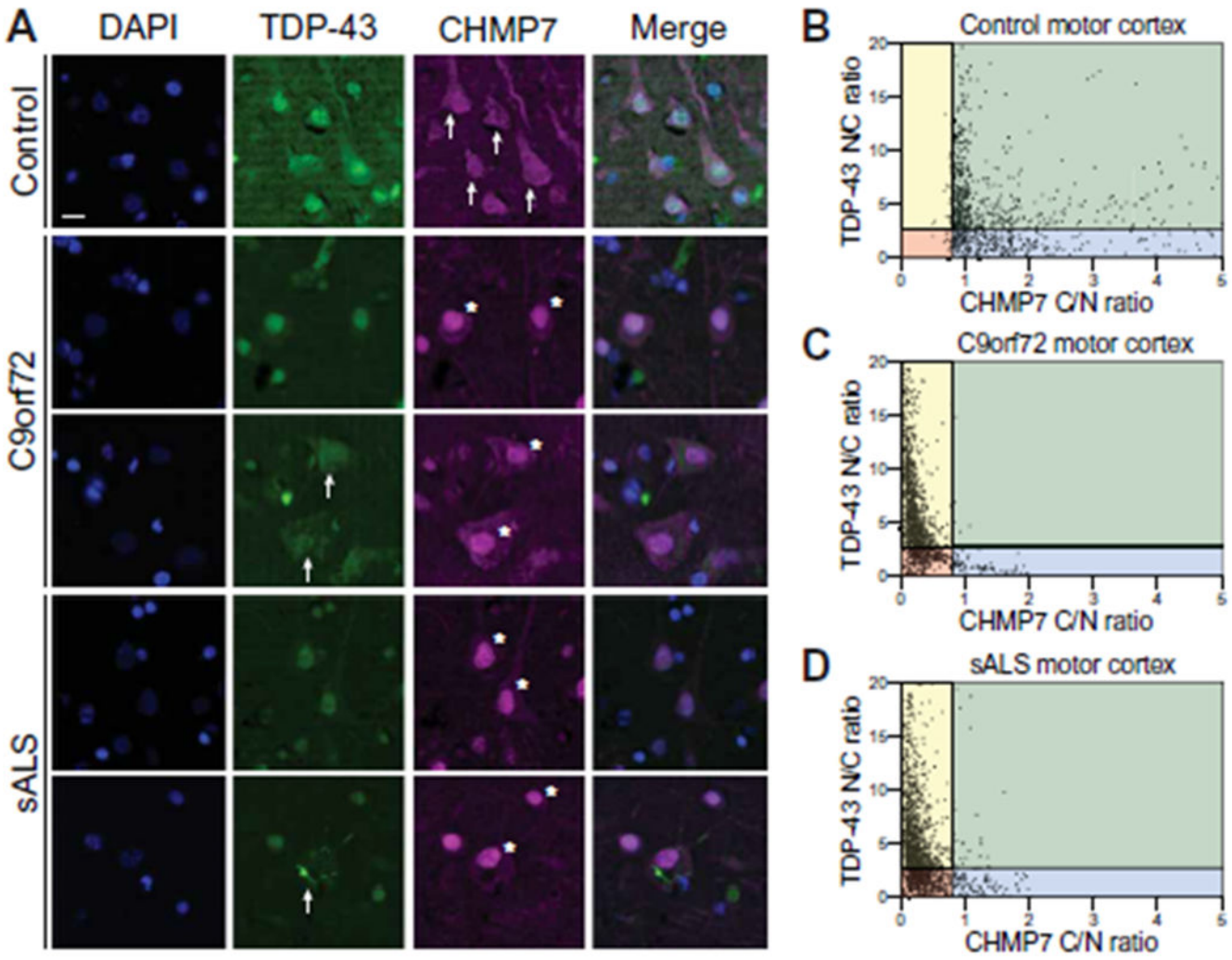

Fig. 5. CHMP7 and TDP-43 co-pathology is present in a subset of neurons in postmortem C9orf72 ALS/FTD and sALS patient motor cortex.

(**A**) Immunostaining for TDP-43 and CHMP7 in paraffin-embedded postmortem motor cortex. Genotype as indicated on left, antibody as indicated on top. Arrows indicate cytoplasmic CHMP7 or TDP-43 immunostaining. Asterisks indicate nuclear CHMP7 immunostaining. (**B** to **D**) Quantification of nuclear/cytoplasmic ratio of TDP-43 versus cytoplasmic/nuclear ratio of CHMP7 in control (B), *C9orf72* (C), and sALS (D) motor cortex. Individual data points for each $Map2^{+}$ neuron analyzed are shown. $n = 10$ control, 10 *C9orf72,* and 20 sALS cases. Note: Red indicates high nuclear CHMP7/low nuclear TDP-43, yellow indicates high nuclear CHMP7/high nuclear TDP-43, blue indicates low nuclear CHMP7/low nuclear TDP-43, and green indicates low nuclear CHMP7/high nuclear TDP-43. Scale bar, 10 μm.

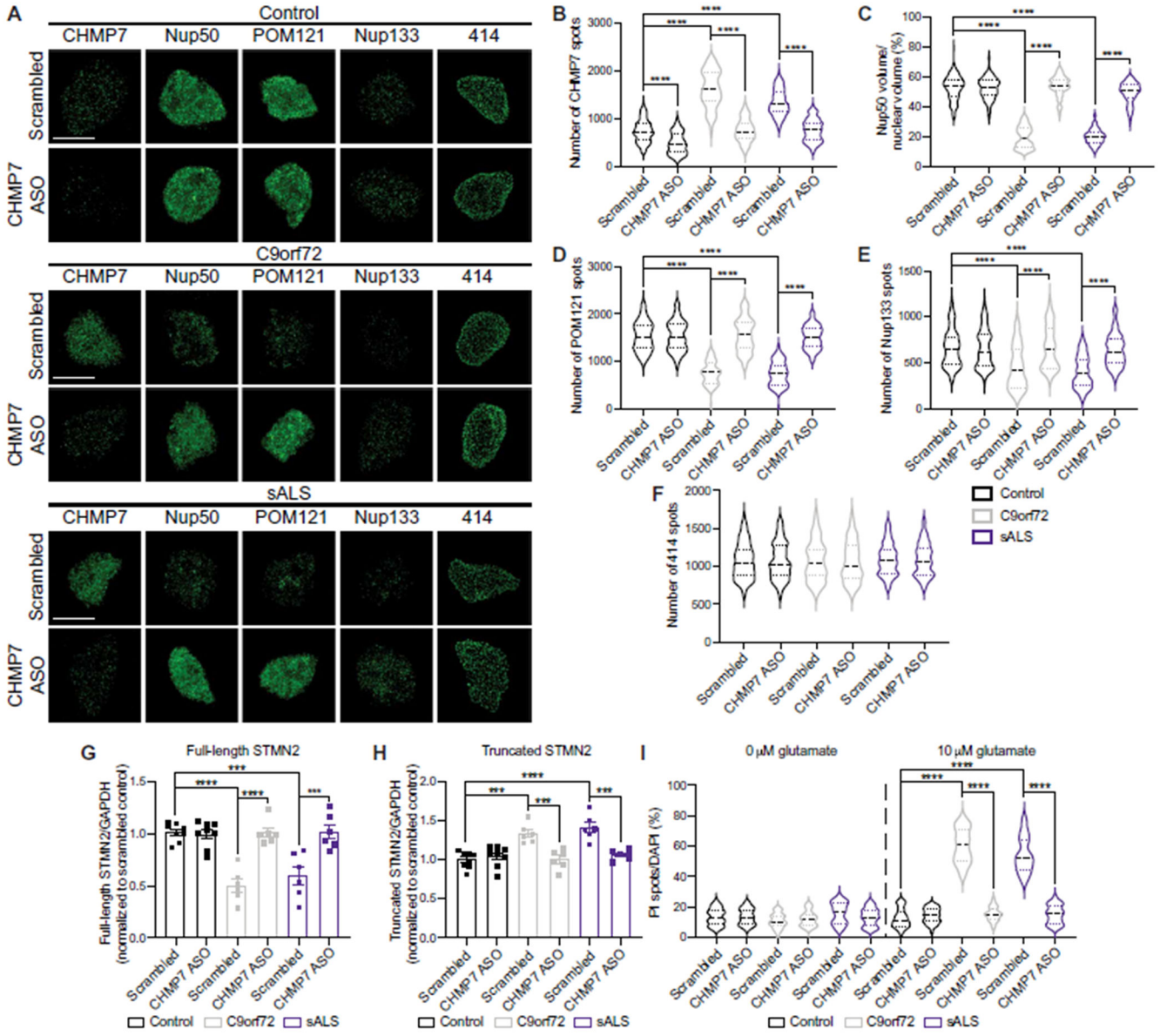

Fig. 6. ASO-mediated knockdown of CHMP7 restores the nuclear expression of specific Nups, mitigates TDP-43-mediated splicing defects, and reduces glutamate-induced excitotoxicity in *C9orf72* and sALS iPSNs.

(**A**) Maximum intensity projections from SIM imaging of nuclei isolated from control, *C9orf72*, and sALS iPSNs on day 40 of differentiation after 2-week exposure to 5 μM scrambled control ASO or CHMP7 ASO 2. Treatment as indicated on left, genotype and antibodies as indicated on top. (**B** to **F**) Quantification of CHMP7 spots (B), Nup50 volume (C), and POM121 (D), Nup133 (E), and 414 (F) spots. $n = 7$ control, 4 *C9orf72*, and 6 sALS iPSC lines, 50 NeuN$^+$ nuclei per line per treatment. Two-way ANOVA with Tukey's multiple comparison test was used to calculate statistical significance. ****$P < 0.0001$. (**G** and **H**) qRT-PCR for full-length (G) and truncated (H) *STMN2* mRNA in control, *C9orf72*, and sALS iPSNs on day 46 of differentiation after 3-week exposure to 5 μM scrambled control ASO or CHMP7 ASO 2. GAPDH was used for normalization. $n = 8$ control, 6

C9orf72, and 6 sALS iPSC lines. Two-way ANOVA with Tukey's multiple comparison test was used to calculate statistical significance. ***$P < 0.001$ and ****$P < 0.0001$. (**I**) Quantification of percent cell death as measured by propidium iodide (PI) incorporation after exposure to glutamate in control and *C9orf72* iPSNs after 2-week exposure to 5 μM scrambled control ASO or CHMP7 ASO 2. $n = 7$ control, 5 *C9orf72,* and 6 sALS iPSC lines, five frames per well. Two-way ANOVA with Tukey's multiple comparison test was used to calculate statistical significance. ****$P < 0.0001$. Scale bar, 5 μm.